

Dear Editors,

5

Thank you very much for considering the manuscript for the review process. We are glad to submit the response in one file as a pdf. The following description will be helpful to understand the reply and modifications in the draft.

- 1) The reviewer comments are presented in “underlined text” format. The response to the reviewer
10 comments is given in the normal text format.
- 2) The changes made in the draft based on the suggestions/comments from the reviewers are highlighted in “red” colour. While the text as “red” colour (was present in the initial discussion manuscript) will be removed in the final revised version.
- 3) The changed/replaced figures are presented in “**red colour rectangle with glow around**”.

15

Please note: the revised version (without any highlighted part) of the manuscript is also uploaded, separately.

“Interactive comment on “Laser induced fluorescence based detection of atmospheric nitrogen dioxide and comparison of different techniques during the PARADE 2011 field campaign” by Umar Javed et al.”

Response: *Umar Javed et al.*

5

“Anonymous Referee #1”

“General comments:”

10 “This manuscript describes a new laser induced fluorescence instrument developed for ground-based and aircraft measurements of NO₂. The authors report the instruments characteristics, laboratory tests, an extensive description of the calibration system, and the first results of a field campaign in 2011, where they carried out an intercomparison with other systems that measured NO₂ using different techniques. The manuscript is generally well written, and the main results of the intercomparison and the description of a new LIF system characteristics, which uses a CW laser is of a certain importance for future developer of NO₂ systems and for the all community working on NO_x measurements. In my opinion it fits with AMT scopes and I recommend publication, after the authors address the following questions and comments.”

15

Response: We are thankful for the Anonymous Referee (#1) for the review and useful comments on the draft.

“Specific comments:”

20 “Lines 52-67: Since the aim of the manuscript is to describe a new NO₂ instruments, and because there are different techniques to measure NO and NO₂, I would limit the review of the measurements techniques to those for NO₂ observation, omitting those for NO detection.”

Response:

We agree with the reviewer. Lines 55-67 (based on the discussion draft) are replace in the revised draft as follows

25 “The Photofragmentation Two-Photon Laser-Induced Fluorescence (PF-TP-LIF) (Sandholm et al., 1990;Bradshaw et al., 1999) and chemiluminescence (Fontijn et al., 1970) methods are well known for direct in situ NO detection. In the past, an indirect detection of NO₂ with these techniques has been performed by converting NO₂ → NO via photolytic/catalytic process followed by NO detection. However, in the case of NO₂ to NO conversion, a potential interference from NO_x species cannot be fully excluded for the NO₂ measurement, e.g. (Crawford et al., 1996;Villena et al., 2012;Reed et al., 2016).”

30 “Line 150-155: I suggest to describe with more details the time-resolved fluorescence signal detection, trigger system, synchronization, how to take care of laser power fluctuation and so on, since this is the key part of the system that may be managed carefully using a CW laser.”

Response:

To explain the data acquisition following “sentences” are included in the draft.

35 “A counter card is used for the data acquisition. There is no need for synchronisation as the counter card itself triggers the laser pulse. The timing system is entirely controlled by an FPGA (field-programmable gate array), utilizing an external crystal oscillator of 20MHz nominal frequency with a stability of +/-2.5ppm over the temperature range of -30°C to +75°C. All internal frequencies are derived from this clock by means of a PLL (phase-locked loop) in the FPGA. The triggering occurs at a fixed rate of 5 Mhz. The delay caused by the length of the trigger cable (propagation delay of the pulse), the laser power supply unit, propagation delays from detector to FPGA, etc. is compensated with a programmable delay for the data acquisition in the FPGA.

40

So the FPGA logic recognizes when it should start recording the data after it emitted the trigger pulse and waits the specified amount of programmed clock cycles after emitting the trigger.”

The signal from the PMT is attained for both periods of the laser cycle (100 ns ON, 100 ns OFF). The card has more than 50 channels available for the PMT data. Each channel has a resolution of 4 ns. The integrated raw data is written in a bin file for the sampling period. The sampling period is typically 1s. The NO₂ fluorescence signal is resolved in the post analysis of the raw data. To elaborate the raw signal, a figure for the time-resolved fluorescence is added as a subpart of ‘Fig. 2’ to the draft.

The power of the diode laser is monitored and recorded continuously/simultaneously by using a photodiode. Later, the NO₂ signal is generally normalized by using the photodiode signal. This is a regular approach for any LIF instrument and has been described previously by many studies. It is noteworthy that the impact of the correction was not significant during the field campaign PARADE. This is because during PARADE-2011, frequent calibrations were performed. So any variability in the power of the laser was captured via the calibration.

“Line 157-265: The calibration system that uses the NO titration by O₃ to produce NO₂ is described and used in different ground-based instruments (i.e. Ryerson et al, 2000, Matsumoto et al., 2000, Osthoff et al., 2006). In my opinion it is a good approach that can be a system for periodical laboratory check of the instrument performance and of the possible NO₂ cylinder degradation, but according also to figure 7 it is the bigger part of the system and includes many components not so compact such as the ozone generator and the ozone analyser. The use of this calibration system seems not easy on ground-based field campaign and really complicated on aircraft.”

Response:

The formation of NO₂ via the gas phase titration is very common approach used for the calibrations of NO_x analysers. A reference to the previous study (Ryerson et al., 2000) is included. We agree with the reviewer that the bigger part of the instrument is the calibration system. However, most parts of the system (like MFCs, valves, reaction chamber, etc.) including the ozone generator is part of a single 19-inch rack mount (4RU). The ozone analyser is also 19-inch rack mount (4RU). So basically, two 19-inch rack mount and a small pump are required for the complete system.

The calibration system can be used to check degradation/changes in the concentration over a period of time in a NO₂ cylinder. We adapted such an approach in the past, but the day to day variation in different NO₂ cylinders was hard to track, since these cylinders showed unstable concentrations with low repeatability even within a short period of time. These checks were performed with different instruments (CLD, CRD, and GANDALF) during different periods of time. In a short time scale (hours), the observed difference was within 3-13% for different NO₂ gas cylinders. Whereas for a longer period (months), the differences were roughly up to 30%. Therefore, to get a reliable signal, the gas phase titration is advantageous compared to the use of a NO₂ cylinder.

“Technical corrections:”

“Line 52: It is quite rare but sometimes NO₂ can be more than 100 ppb so I would replace ‘100’ with ‘hundreds’. Line 73: Add ‘the’ between ‘in’ and ‘past’.”

Response:

Replacement is added.

“Line 74: remove the subscript to the ‘v’ of pptv.”

Response:

It is done.

85 “Line 79: The reference reported (Dari-Salisburgo et al, 2009) describes the first ground-based system developed by that group. I suggest to substitute this reference with the work of the same group (Di Carlo et al., 2013) that reports the evolution of their TD-LIF for aircraft measurements that has better sensitivity and performances.”

Response:

Added the reference “(Di Carlo et al., 2013)” at this position.

90 “Line 182: Remove ‘Figure 3’ ”

Response:

It is done.

95 “Line 710 (Table 1): I would include the evolution of the instrument described by Dari-Salisburgo et al, 2009, used also for aircraft measurements, because it uses another laser a Nd:YVO4 pulse laser, and has better performance in terms of LOD compared with that described in Dari-Salisburgo et al, 2009, more details can be found in Di Carlo et al., 2013.”

Response:

The successor instrument is indeed better in sensitivity from the predecessor. The overview of the instrument described in (Di Carlo et al., 2013) is also added to Table 1 as suggested by the reviewer.

100

References

- 105 Bradshaw, J., Davis, D., Crawford, J., Chen, G., Shetter, R., Muller, M., Gregory, G., Sachse, G., Blake, D., Heikes, B., Singh, H., Mastromarino, J., and Sandholm, S.: Photofragmentation two-photon laser-induced fluorescence detection of NO₂ and NO: Comparison of measurements with model results based on airborne observations during PEM-Tropics A, *Geophys Res Lett*, 26, 471-474, Doi 10.1029/1999gl900015, 1999.
- Crawford, J., Davis, D., Chen, G., Bradshaw, J., Sandholm, S., Gregory, G., Sachse, G., Anderson, B., Collins, J., Blake, D., Singh, H., Heikes, B., Talbot, R., and Rodriguez, J.: Photostationary state analysis of the NO₂-NO system based on airborne observations from the western and central North Pacific, *J Geophys Res-Atmos*, 101, 2053-2072, Doi 10.1029/95jd02201, 1996.
- 110 Di Carlo, P., Aruffo, E., Busilacchio, M., Giammaria, F., Dari-Salisburgo, C., Biancofiore, F., Visconti, G., Lee, J., Moller, S., Reeves, C. E., Bauguitte, S., Forster, G., Jones, R. L., and Ouyang, B.: Aircraft based four-channel thermal dissociation laser induced fluorescence instrument for simultaneous measurements of NO₂, total peroxy nitrate, total alkyl nitrate, and HNO₃, *Atmos Meas Tech*, 6, 971-980, 10.5194/amt-6-971-2013, 2013.
- 115 Fontijn, A., Sabadell, A. J., and Ronco, R. J.: Homogeneous Chemiluminescent Measurement of Nitric Oxide with Ozone - Implications for Continuous Selective Monitoring of Gaseous Air Pollutants, *Anal Chem*, 42, 575-579, Doi 10.1021/Ac60288a034, 1970.
- Reed, C., Evans, M. J., Di Carlo, P., Lee, J. D., and Carpenter, L. J.: Interferences in photolytic NO₂ measurements: explanation for an apparent missing oxidant?, *Atmos. Chem. Phys.*, 16, 4707-4724, 10.5194/acp-16-4707-2016, 2016.
- 120 Ryerson, T. B., Williams, E. J., and Fehsenfeld, F. C.: An efficient photolysis system for fast-response NO₂ measurements, *J Geophys Res-Atmos*, 105, 26447-26461, Doi 10.1029/2000jd900389, 2000.
- Sandholm, S. T., Bradshaw, J. D., Dorris, K. S., Rodgers, M. O., and Davis, D. D.: An Airborne Compatible Photofragmentation 2-Photon Laser-Induced Fluorescence Instrument for Measuring Background Tropospheric Levels of No, Nox, and No₂, *J Geophys Res-Atmos*, 95, 10155-10161, DOI 10.1029/JD095iD07p10155, 1990.

125 Villena, G., Bejan, I., Kurtenbach, R., Wiesen, P., and Kleffmann, J.: Interferences of commercial NO₂ instruments in the urban atmosphere and in a smog chamber, *Atmospheric Measurement Techniques*, 5, 149-159, DOI 10.5194/amt-5-149-2012, 2012.

“Interactive comment on “Laser induced fluorescence based detection of atmospheric nitrogen dioxide and comparison of different techniques during the PARADE 2011 field campaign” by Umar Javed et al.”

Response: *Umar Javed et al.*

5

“Anonymous Referee #2”

“The manuscript of Umar Javed and colleagues is an interesting study on a new laser induced fluorescence instrument for the measurement of atmospheric nitrogen dioxide. It describes the set-up of this instrument with an emphasis on its calibration system and the analysis of possible cross-sensitivities. An important part of the manuscript focuses on the results of an intercomparison field campaign where different nitrogen dioxide measurement techniques have been compared. Nitrogen dioxide is an important atmospheric trace gas and imposes quite some efforts to perform good measurements with different techniques. This manuscript makes a valuable contribution to improve nitrogen dioxide measurement techniques. I recommend this manuscript for publication; however there are some points that should be addressed before.”

15 **Response:** We appreciate the time given by the Anonymous Referee (#2) for the review. The helpful comments of the reviewer will provide more clarity to the draft.

“Specific comments:”

20 **L16:** Abstract: I suggest that in the abstract the field campaign PARADE should be mentioned; also the location and time of the field campaign.”

Response:

The name of the campaign along location and time is added in the abstract.

L 32: Aircraft emissions as well are directly affecting the free troposphere.”

25 **Response:**

Aircraft emissions, as a source for the NO_x in the upper troposphere (Strand and Hov, 1996), are included.

L 96: The wavelength of the laser is given but not the wavelength of the fluorescence.”

Response:

30 The NO₂ fluorescence has a broad spectrum. It starts at the excitation wavelength and extends into the infra-red region (Wehry, 1976). But still, the major fraction of the fluorescence still lies in the visible region (Sakurai and Broida, 1969; Sugimoto et al., 1982). In our case, we block the light with the interference filter at wavelengths < 550 nm. The cut-off band of the PMT is at about 890 nm. So the wavelength range of the detection window of the fluorescence signal is roughly between 550-890 nm. Still, we expect the major portion would be in the visible region. This is already explained in the text, so we have added also the lower
35 limit “ $\lambda \geq 449\text{nm}$ ” for the emitted fluorescence in “R.2”.

L 103: In this context: What is the definition of zero air?”

Response:

40 The zero air is Synthetic air (hydrocarbon-free) as specified by Westfalen (99,999 mol% pure mixture of 20.5% O₂ in N₂, H₂O < 5 ppmv, HC < 0.1 ppmv, NO_x < 0.1 ppmv). Some studies e.g., (Thieser et al., 2016) showed that it is not fully free of NO₂

contamination, though levels are generally much smaller than the 0.1 ppmv specified. They estimate up to 20 ppt NO₂ in their supply of synthetic air cylinders. The Synthetic air was used during the PARADE field campaign for the background measurements of our instrument. The quality of the air is discussed in the section 3 (related to PARADE) of the draft.

45 Ideally, the zero air should be a replica of ambient-air but without the NO₂. In the past, it has been tried to use scrubbing techniques, based on active charcoal, coated surface with a certain chemical etc., to remove NO₂ from the ambient-air and use the scrubbed air for the background measurements (Matsumoto and Kajii, 2003). This can be done for a lower sampling rate, but at our high sampling flow rates (>4SLM) oversized scrubbing filters would be required to provide sufficient residence times.

50 “L 125 / L 144: What is the PMT temperature? Is the PMT actively cooled? What causes the background signal? Would the background decrease, if the PMT was cooled down at temperatures below 0°C by an active cooling unit?”

Response:

55 The internal temperature of the PMT is 0°C. It is regulated by a built-in thermoelectric cooler and this feature is part of the hardware from the manufacturer. We only have the control to regulate the surface temperature of the PMT. This is done externally by using a water chiller at 20°C or 25°C (avoiding condensation) according to manufacturer recommendations. The dark counts on the PMT signal are generally less than 50 counts s⁻¹ for the channels used for the NO₂ fluorescence detection. The major reason for the background signal, larger than the dark signal typically by a factor >25, is expected to be fluorescence contamination from the Herriot cell mirrors existing in the red region of wavelength.

60 “L 223: “. . . at a lower temperature . . .” Which temperature?”

Response:

The sentence was to give a general statement.

65 Under lower temperature conditions, the reaction between NO and O₃ slows down. This can lead to a change in the conversion efficiency from NO to NO₂. In our case, many electrical parts (electronic valves, ozone generator, and mass flow controllers) are installed inside the calibration unit. In a fully operational mode for one day, the temperature build up in the calibration unit is 8-10°C higher than ambient temperatures. From our experience/observations, conditions with a temperature lower than 20°C inside the calibrator do not occur.

“L 237: Is there an explanation for the change in sensitivity? What is the range of sensitivity change?”

Response:

70 Generally, some factors can contribute to a change in the sensitivity e.g., stability of the optics alignment, cleanness of the optics, temperature related effect of electronics, stability of the calibration signal etc. Frequent calibrations were performed during the PARADE-2011 to assess the stability of the sensitivity. Based on calibrations (> 130) performed during PARADE-2011 by using dry-air (< 25 ppm of water), the relative variation in the sensitivity of the instrument was better than ± 2.7 % (1σ). Further, the sensitivity of the instrument decreases by 5 % (relative to the dry-air) at 1 % of atmospheric H₂O vapour. This is corrected by using simultaneous measurement of H₂O vapour.

80 “L 268: Figure 8 shows the relative precision obtained during different calibrations. But how exactly do you determine the relative precision? Does it include for example only the variability of the sensitivity or the variability of the background, etc.? Please describe in more detail.”

Response:

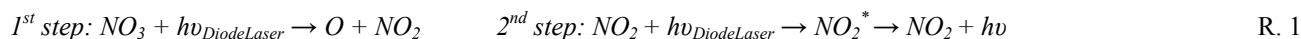
The text in this section of the draft is simplified and the figure is now presented as a function of NO₂ mixing ratios. The relative precision 0.5 % (1 min⁻¹) was calculated based on the standard deviation of the PMT NO₂-signal (in s⁻¹ time resolution) during the calibration period for different NO₂ concentrations. Since the selected signals were based on higher levels of NO₂ concentrations (> 0.5 ppb). So the number 0.5 % (1 min⁻¹) is true representative of precision at higher NO₂ concentrations.

85 Standard deviation of signals at different NO₂ concentrations can be extrapolated to zero for determination of the precision at background level. It can also be calculated from the standard deviation of the zero-air signal. Both approaches give a similar result of about 3 ppt precision for our instrument. Hence, the total precision was defined by considering the both values i.e., 0.5% (1 min⁻¹) + 3 ppt (1σ).

90 “L 318: R6 is not a valid chemical reaction (both sides of the reaction arrow should be balanced).”

Response:

It is modified as follows



95 “L 337: I agree the short residence time of the sample air inside the instruments minimizes the thermal decomposition of the respective species. But please give at least a few calculated lifetimes against thermal decomposition for the most important interfering gases that illustrate this statement.”

Response:

At this line, the discussion was referring to the sampling line prior to the orifice. This information is further clarified in the text.

100 The ambient lifetime based on thermal decomposition is added for different species. The lifetime inside the instrument would be much larger as the cell pressure is about a factor 100 smaller compared to the ambient pressure.

“L505: I suggest that in the summary the authors underline the main advantage and disadvantage of this measuring system, also in comparison with other measurement techniques. What is the future of Gandalf (besides LOTR)? Are there specific plans to use this instrument during other field campaigns?”

105

Response:

Following “sentences” are included in the summary of the draft.

“In general, all instruments performed well. GANDALF showed a very good correlation ($R^2 \approx 0.99$) in comparison to other in situ instruments (Fig. S11 in the supplement) and even with LP-DOAS the correlation was $R^2 \approx 0.9$. The differences in the absolute values were within the specified range of individual measurement errors. The main advantages and disadvantages of GANDALF compared to the other instruments are summarized as follows.

110

In comparison to the CRDS instrument, the main advantage for GANDALF is that the sampling can be achieved without an inlet-line. This is not possible for the close-path CRDS system. This provides the capability of the detection at ambient temperature for GANDALF, which is especially of an advantage for aircraft measurements of NO₂ where avoiding interference from CH₃OONO₂ and HO₂NO₂ (via unwanted thermal dissociation) is very important. The requirement of calibration is the main disadvantage for GANDALF compared to CRDS (absolute technique). However, both instruments require frequent zero-air measurements. The limit of detection for both instruments was of similar magnitude during PARADE-2011.

115

The CE-DOAS instrument is comparable to the CRDS instrument. It also needs frequent background measurements but no absolute calibration. GANDALF has a much better in the sensitivity compared to the CE-DOAS instrument. During PARADE-2011, the detection limit for CE-DOAS was around 300 ppt (2σ, 30 s) while for GANDALF the detection limit was

120

5 – 10 ppt (min^{-1}). A low-cell-pressure is typically required to achieve a good sensitivity for LIF instruments (Table 1) while the detection in the other instruments (CRDS and CE-DOAS) is performed at sub-ambient pressures (>800 hPa). The requirement of calibration and usage of a larger scroll-pump (to achieve a low-cell-pressure) adds extra effort/cost to the GANDALF measurements.

125 The basic requirements for a calibration and background measurements are same in CLD and GANDALF. In the case of CLD, the maintenance is relatively easy compared to GANDALF. But GANDALF provides a direct detection of NO_2 compared to the indirect detection of NO_2 (via $\text{NO}_2 \rightarrow \text{NO}$) in the CLD instrument. The sensitivity of GANDALF was better than the CLD instrument during PARADE-2011.

130 LP-DOAS does not require calibration or the zero-air measurement. For this reason, the uncertainty of the data is also very small compared to GANDALF or other in situ measurements. This is the main advantage of the LP-DOAS instrument over GANDALF. The restriction of this method is that it does not provide a local measurement. Also, the temporal resolution is limited compared to other in situ instruments. The sensitivity of the LP-DOAS instrument generally depends on the length of a light path, and variations in visibility. It was on average about 0.11 ppb (2σ , 11 s) during PARADE-2011.

Outlook: NO_2 in the free troposphere is variable (seasonally) and generally lower than 50 ppt (Gil-Ojeda et al., 2015). Depending on the location, in the free troposphere and the marine boundary layer, NO_2 can be as low as a few ppt (Beygi et al., 2011;Schreier et al., 2016). These NO_2 ranges are below the detection limit for the instrument (GANDALF) for short time resolutions of 1s, for example. Improvements for future use on aircraft are possible by further reducing the background of the instrument. Since most of the background signal is from the fluorescence contamination of the Herriot's cell mirrors, this could be avoided by using a single beam (as demonstrated by (Di Carlo et al., 2013)) of the laser for detection without a Herriott cell or
140 by using different coatings on the Herriott cell mirrors to increase reflectivity and reduce fluorescence. The current CW diode laser of the instrument may be replaced by an already available mono-mode dual diode laser [λ (online) = 445 nm and λ (offline) = 442 nm] for on and off resonance measurements of NO_2 . Replacement of current laser to the dual diode laser will decrease partially the dependency on the frequent zero-air background measurements.

The formation of RONO_2 is an important sink for NO_x and effects the ozone production efficiency (Browne and Cohen, 2012). The accurate measurement of RONO_2 is important for the assessment of local O_3 abundances. LIF systems in combination with the thermal dissociation method (Day et al., 2002) are also used and very useful for the detection of RONO_2 , RONO_2 , and HNO_3 . GANDALF will be capable (currently under development) of measuring these species by coupling with the thermal dissociation inlets. This further development could provide very useful data for the future to constrain models.”

150
“L 508: The authors are mentioning that the instrument is capable for measurements throughout the troposphere with a time resolution of 1 s to 1 min. However, the whole preceding discussion has been focused on ground based measurements at a time resolution of 1 min. Also the concentration of NO_2 in the free troposphere is much lower than in the boundary layer. LOD would increase significantly if you reduced the sampling time from 60 s to 1s. Please outline in short what improvements would be necessary to achieve this goal.”

Response:

NO_2 in the free troposphere is variable (seasonally) and generally lower than 50 ppt (Gil-Ojeda et al., 2015). Depending on the location, in the free troposphere and the marine boundary layer, NO_2 can be as low as a few ppt (Beygi et al., 2011;Schreier et al., 2016). These NO_2 ranges are below the detection limit for the instrument for short time resolutions of 1s, for example.
160 Improvements for future use on aircraft are possible by further reducing the background of the instrument. Since most of the

background signal is from the fluorescence contamination of the Herriot's cell mirrors, this could be avoided by using a single beam (as demonstrated by (Di Carlo et al., 2013)) of the laser for detection without a Herriott cell or by using different coatings on the Herriott cell mirrors to increase reflectivity and reduce fluorescence.

165

“Technical Corrections:”

“L 298: . . . about 8 time higher than the cross section of . . .”

Response:

170 It is done.

“Tables:”

“Table 3: $\pm\delta$ – explanation in the caption is missing.”

175 **Response:**

It is done.

“Table 4: Uncomplete caption - which ratios?”

Response:

180 It is modified as follows.

“Average the ratios of NO₂ measurements from the different instruments, taking into account all available data from PARADE-2011.”

185

“Figures:”

“In general the figure captions are often not sufficient in explaining the content of the figures.”

190 **“Figure 1: The numbers in the caption of this figure have different orientations and do not facilitate the reading. All numbers should have the same conventional orientation (like the numbers “9, 10, . . .”?. “SF” - This is not quite consistently. All other objects of this figure stand for units of the instrument. “Sampling flow” is the gas stream into the instrument (I assume) and not part of the instrument. So it would be more suitable to write: Inlet orifice or sampling flow line, or”**

Response:

The numbering in the figure/text is simplified, and synchronized.

195

“Figure 4: . . . as a function of O₃ concentration in . . . Please explain “arb” in the y-axis label. The caption is incomplete; “Box-Model NO₂” is not mentioned.”

Response:

It is modified as follows.

200 “The PMT NO₂ signals in counts (cts) are shown as a function of O₃ concentrations in the calibrator (y-axis scale on the left side), together with NO₂ calculated from a box model of the NO₂ production in the calibrator (y-axis scale on the right side).”

“Figure 5: “also theoretically calculated residence time (7.73s). . .” I assume the red line in this figure is meant.”

Response:

205 Yes, the red line is showing the theoretical residence time. This information is now added to the caption in the draft.

“Figure 6: What do you mean by calibration signal? I assume it is the number of counts at the PMT?”

Response:

210 Yes, these are counts at the PMT. It is corrected in the caption.

“L 250 – L 265 / Figure 7: The description in the text and in the figure caption is a little bit confusing and should be clarified. E.g. an ozone analyzer is shown in the figure but not mentioned in the text. In the text blue, red and white arrows are mentioned; in the figure you find additionally orange arrows. In the text only red arrows in L2 are mentioned, but there also white arrows found in L2. I assume that the valves EV3 and EV2 have to point at the position P1(P2) at the same time? Above the Gandalf-box in Figure 7 there are three times written “4100 sscm” in different colors and different orientation. As long as you do not discuss it explicitly in the text, one “4100 sscm” label is enough. Figure caption: “outdoor – operations”? - Better during field campaigns or during the PARADE field campaign.”

220 **Response:**

The ozone analyser is used to check the concentration of O₃ in the calibration gas, and this information is now included in the text. The orange arrow has been removed. The white arrow was representing ambient air flow during along the overflow of the calibration gas. P1 and P2 where switched around. The figure has been revised along with the text to correct it and make it easier to understand in the updated version of the draft.

225

“Figure 8: JD = Julian Days. The formulation of this caption is a little bit unclear. Please improve.”

Response:

230 The relative precision in this figure is now shown as a function of NO₂ mixing ratios instead of time. The caption of the figure is also accordingly changed.

“Figure 12 and 13: “Ratios. . .” – The readability would be improved if you would write in the caption which ratio is meant. Please choose the same y-scale for all figures.”

Response:

235 All the figures are modified for as suggested by the reviewer.

References:

- 240 Beygi, Z. H., Fischer, H., Harder, H. D., Martinez, M., Sander, R., Williams, J., Brookes, D. M., Monks, P. S., and Lelieveld, J.: Oxidation photochemistry in the Southern Atlantic boundary layer: unexpected deviations of photochemical steady state, *Atmos Chem Phys*, 11, 8497-8513, 10.5194/acp-11-8497-2011, 2011.
- Browne, E. C., and Cohen, R. C.: Effects of biogenic nitrate chemistry on the NO_x lifetime in remote continental regions, *Atmos Chem Phys*, 12, 11917-11932, 2012.
- 245 Day, D. A., Wooldridge, P. J., Dillon, M. B., Thornton, J. A., and Cohen, R. C.: A thermal dissociation laser-induced fluorescence instrument for in situ detection of NO₂, peroxy nitrates, alkyl nitrates, and HNO₃, *J Geophys Res-Atmos*, 107, ArtN 4046
10.1029/2001jd000779, 2002.
- 250 Di Carlo, P., Aruffo, E., Busilacchio, M., Giammaria, F., Dari-Salisburgo, C., Biancofiore, F., Visconti, G., Lee, J., Moller, S., Reeves, C. E., Bauguitte, S., Forster, G., Jones, R. L., and Ouyang, B.: Aircraft based four-channel thermal dissociation laser induced fluorescence instrument for simultaneous measurements of NO₂, total peroxy nitrate, total alkyl nitrate, and HNO₃, *Atmos Meas Tech*, 6, 971-980, 10.5194/amt-6-971-2013, 2013.
- Gil-Ojeda, M., Navarro-Comas, M., Gomez-Martin, L., Adame, J. A., Saiz-Lopez, A., Cuevas, C. A., Gonzalez, Y., Puentedura, O., Cuevas, E., Lamarque, J. F., Kinninson, D., and Tilmes, S.: NO₂ seasonal evolution in the north subtropical free troposphere, *Atmos Chem Phys*, 15, 10567-10579, 2015.
- 255 Matsumoto, J., and Kajii, Y.: Improved analyzer for nitrogen dioxide by laser-induced fluorescence technique, *Atmos Environ*, 37, 4847-4851, 10.1016/j.atmosenv.2003.08.023, 2003.
- Sakurai, K., and Broida, H. P.: Spectral Study of No₂ Fluorescence Excited by 11 Lines of Argon and Krypton Ion Lasers, *J Chem Phys*, 50, 2404-&, Doi 10.1063/1.1671395, 1969.
- 260 Schreier, S. F., Richter, A., Wittrock, F., and Burrows, J. P.: Estimates of free-tropospheric NO₂ and HCHO mixing ratios derived from high-altitude mountain MAX-DOAS observations at midlatitudes and in the tropics, *Atmos Chem Phys*, 16, 2803-2817, 10.5194/acp-16-2803-2016, 2016.
- Strand, A., and Hov, O.: The impact of man-made and natural NO_x emissions on upper tropospheric ozone: A two-dimensional model study, *Atmos Environ*, 30, 1291-1303, Doi 10.1016/1352-2310(95)00413-0, 1996.
- 265 Sugimoto, N., Takezawa, S., and Takeuchi, N.: Time-Resolved, Dispersed Laser-Induced Fluorescence of NO₂ - Observation of Collision-Induced Energy-Transfer Effect, *Jpn J Appl Phys* 1, 21, 1536-1538, Doi 10.1143/Jap.21.1536, 1982.
- Thieser, J., Schuster, G., Schuladen, J., Phillips, G. J., Reiffs, A., Parchatka, U., Pöhler, D., Lelieveld, J., and Crowley, J. N.: A two-channel thermal dissociation cavity ring-down spectrometer for the detection of ambient NO₂, RO₂NO₂ and RONO₂, *Atmos Meas Tech*, 9, 553-576, 10.5194/amt-9-553-2016, 2016.
- 270 Wehry, E. L.: Modern fluorescence spectroscopy, *Modern analytical chemistry*, Plenum Press, New York, v. <1-4 > pp., 1976.

“Interactive comment on “Laser induced fluorescence based detection of atmospheric nitrogen dioxide and comparison of different techniques during the PARADE 2011 field campaign” by Umar Javed et al.”

Response: Umar Javed et al.

5

“Anonymous Referee #3”

10 “This manuscript describes a laser induced fluorescence instrument that has been developed for ground and aircraft based measurements of NO₂. It describes the setup of the instrument, its calibration and examines possible interferences. There is also a description of data taken with the instrument during a field campaign that involved a range of different NO₂ detection techniques and a comparison of the different datasets is made. NO₂ is a key atmospheric constituent and it is important to develop new direct measurement techniques for it, making this type of work very topical. The manuscript is generally well written and provides an important reference for others wishing to develop an LIF instrument for NO₂ detection. I recommend publication subject to the authors dealing with the following relatively minor comments.”

15 **Response:** We are grateful for the Anonymous Referee (#3) for accepting the draft for the review and giving time for the useful comments on the draft.

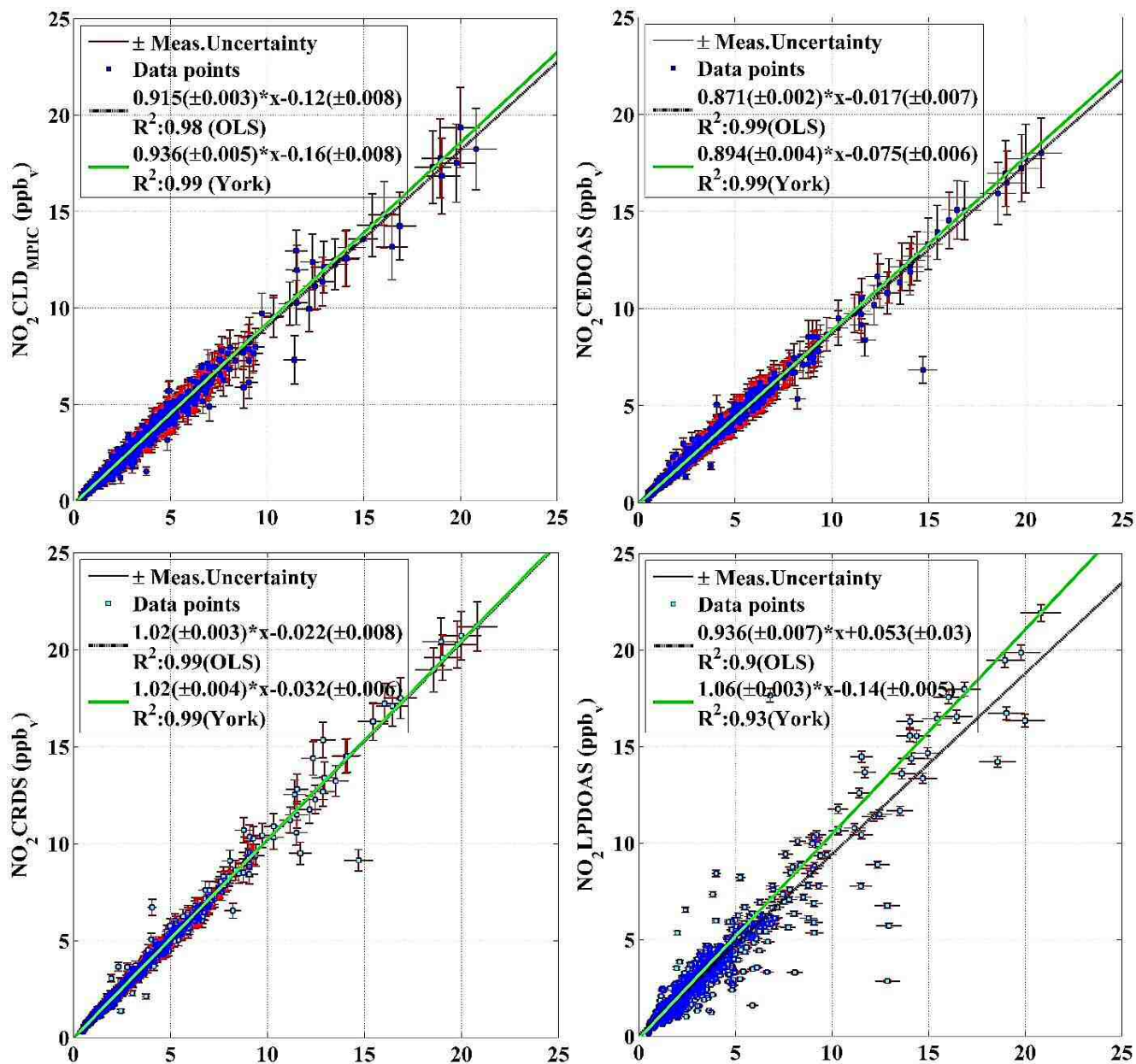
“Specific comments:”

20 “On line 254 it is stated that frequent zero-air measurements are necessary to monitor changes in the background signal. This is important as presumably the addition of air with zero NO₂ in it is the only way that the background signal of the instrument can be measured? I therefore think that more discussion should be had into this. Firstly, how is the zero air generated, is it just from a cylinder or is there some further scrubbing carried out? How do the authors know how much NO₂ is in their zero air, has it been measured? Some discussion should be had as to how the quality of the zero air effects the accuracy of the instrument.”

25 **Response:**

Yes, the zero NO₂ (zero air) measurements were the only way to determine the background of the instrument for the setup used in PARADE-2011. The zero air was directly used from the cylinder (Synthetic air, hydrocarbon free) without any extra scrubbing method. The discussion about the zero air is part of the PARADE-2011 field campaign. It is described in the section “3.1 NO₂ inter-comparison during PARADE (‘GANDALF’)”. For the gas supply, a gas bundle (12 × 50 L × ~200bar) was used during the campaign. We did not know the absolute value of NO₂ in the zero air for PARADE-2011. However, we observed differences of up to ± 8 ppt in 70 % (1σ) of the hourly based successive background measurements (> 500). This variability can be a good indicator for the uncertainty in the zero air. A NO₂-contamination in zero air will not impact the precision of the instrument but (accuracy) it would lead to underestimate the ambient NO₂.

35 Another indication that the NO₂ contamination in zero air used during PARADE-2011 was less than GANDALF’s detection limit is that in the data analysis the y-intercept of other NO₂ in situ instruments (y-axis) vs GANDALF (x-axis) showed always a negative number. If the GANDALF zero-measurements would have significant NO₂ contamination the y-intercept should be positive.



40

Figure 1: The individual correlation of different NO₂ instruments (y-axis) versus GANDALF (x-axis) is shown for available 10 minutes data averages. The two different fitting procedures i.e. based on least square fit (Bevington and Robinson, 1992) and York method (York et al., 2004) are applied.

45

"In the instrument description section I feel that a diagram showing the timing of the laser pulse, PMT detection and fluorescence signal would be beneficial. All the information is there in the paragraph but a diagram would makes things much clearer."

Response:

50

A figure (Fig. S4) showing the raw data for the laser cycle was provided in the supplement of the draft. We have transferred (with modification) this figure from supplement to the main draft as part of the "Fig. 2".

55 “On line 144 it is stated that the PMT and laser are kept at a constant temperature by a water chiller but at what temperature? Would lowering the temperature help with reducing background? Or conversely if no cooling was present, which may make the instrument easier to operate on an aircraft, how would this affect instrument performance?”

Response:

60 The surface temperature of the PMT and laser is kept at a temperature of 20°C or 25°C (avoiding condensation) by circulating water. This provides the heat sink for the internal thermoelectric cooling of the PMT (@ 0°C) and laser (@ 25°C). The internal cooling is the default setting from the manufacturer.

65 The internal temperature cannot be regulated by an external cooling. The external temperature should be in the range of 5-35°C along a sufficient heat exchange system (fan cooling, water circulation etc.). Moreover, the dark counts on the PMT signal are in the order of $< 50 \text{ counts s}^{-1}$ for the channels used for the NO₂ fluorescence detection. The major reason for the background signal, larger than the dark signal typically by a factor >25 , is expected to be fluorescence contamination from the Herriot cell mirrors existing in the red region of wavelength. For a stable (parameters like power, wavelength, shape of the beam etc.) laser operation, an external temperature range is within 15-30°C. This range is sufficient to keep the internal temperature of the laser at 25°C. A laser operation out of the specified range would lead to shut-off/potentially damage the laser.

70 “On line 199 it is stated that in the calibration system, about 99% of the NO is consumed by titration with O₃ to produce the NO₂. Why do the authors choose to titrate this much? Surely there is a danger that they could have more O₃ than NO in the system and hence have the potential for secondary chemistry to affect the amount of NO₂ present? Would it not be better to titrate around 80% of the NO to NO₂?”

Response:

75 The secondary chemistry will always be present (from the beginning) regardless of a partial or full titration. Only the net impact would be larger/smaller with full/partial titration, respectively. Our model simulations/lab experiments have shown that the impact of secondary chemistry in our system was only around 1 %. These results were discussed in the earlier section (lines 178-195) of the submitted draft.

80 “In the abstract it is stated that the instrument could be used for airborne measurements of NO₂ however there is very little discussion of this in the manuscript. There should at least be some discussion as to how the instrument precision and detection limit would change for 1 second averaging (which would be required for aircraft work) and how this compares to the potentially lower levels of NO₂ present in the free troposphere.”

Response:

85 The following “discussion” is included in to the summary of the paper.

90 “NO₂ in the free troposphere is variable (seasonally) and generally lower than 50 ppt (Gil-Ojeda et al., 2015). Depending on the location, in the free troposphere and the marine boundary layer, NO₂ can be as low as a few ppt (Beygi et al., 2011;Schreier et al., 2016). These NO₂ ranges are below the detection limit for the instrument for short time resolutions of down to 1s. Improvements for future use on aircraft are possible by further reducing the background of the instrument. Since most of the background signal is from the fluorescence contamination of the Herriot’s cell mirrors, this could be avoided by using a single beam (as demonstrated by (Di Carlo et al., 2013)) of the laser for detection without a Herriott cell or by using different coatings on the Herriott cell mirrors to increase reflectivity and reduce fluorescence.”

“Technical:”

95

“Figure 1: It would be clearer if the numbers were all the same way up on the page.”

Response:

In the revised version of the draft, the numbers are synchronized with the text as suggested by the reviewer.

100 **“Reaction 2: what is the wavelength of the fluorescence?”**

Response:

The NO₂ fluorescence has a broad spectrum. It starts near the excitation wavelength and extends into the infra-red region (Wehry, 1976). But still, the major fraction of the fluorescence still lies in the visible region (Sakurai and Broida, 1969; Sugimoto et al., 1982). In our case, we block the light with the interference filter until 553 nm. The cut-off band of the PMT is at about 890 nm. So the wavelength range of the detection window of the fluorescence signal is roughly between 553-890 nm. Still, we expect the major portion would be in the visible region. So we have added only the lower limit “ $\lambda \geq 449nm$ ” for the fluorescence in “R.2”.

110

References

- 115 Bevington, P. R., and Robinson, D. K.: Data reduction and error analysis for the physical sciences, 2nd ed., McGraw-Hill, New York, xvii, 328 p. pp., 1992.
- Beygi, Z. H., Fischer, H., Harder, H. D., Martinez, M., Sander, R., Williams, J., Brookes, D. M., Monks, P. S., and Lelieveld, J.: Oxidation photochemistry in the Southern Atlantic boundary layer: unexpected deviations of photochemical steady state, *Atmos Chem Phys*, 11, 8497-8513, 10.5194/acp-11-8497-2011, 2011.
- 120 Di Carlo, P., Aruffo, E., Busilacchio, M., Giammaria, F., Dari-Salisburgo, C., Biancofiore, F., Visconti, G., Lee, J., Moller, S., Reeves, C. E., Bauguitte, S., Forster, G., Jones, R. L., and Ouyang, B.: Aircraft based four-channel thermal dissociation laser induced fluorescence instrument for simultaneous measurements of NO₂, total peroxy nitrate, total alkyl nitrate, and HNO₃, *Atmos Meas Tech*, 6, 971-980, 10.5194/amt-6-971-2013, 2013.
- 125 Gil-Ojeda, M., Navarro-Comas, M., Gomez-Martin, L., Adame, J. A., Saiz-Lopez, A., Cuevas, C. A., Gonzalez, Y., Puentedura, O., Cuevas, E., Lamarque, J. F., Kinnison, D., and Tilmes, S.: NO₂ seasonal evolution in the north subtropical free troposphere, *Atmos Chem Phys*, 15, 10567-10579, 2015.
- Sakurai, K., and Broida, H. P.: Spectral Study of No₂ Fluorescence Excited by 11 Lines of Argon and Krypton Ion Lasers, *J Chem Phys*, 50, 2404-&, Doi 10.1063/1.1671395, 1969.
- Schreier, S. F., Richter, A., Wittrock, F., and Burrows, J. P.: Estimates of free-tropospheric NO₂ and HCHO mixing ratios derived from high-altitude mountain MAX-DOAS observations at midlatitudes and in the tropics, *Atmos Chem Phys*, 16, 2803-2817, 10.5194/acp-16-2803-2016, 2016.
- 130 Sugimoto, N., Takezawa, S., and Takeuchi, N.: Time-Resolved, Dispersed Laser-Induced Fluorescence of NO₂ - Observation of Collision-Induced Energy-Transfer Effect, *Jpn J Appl Phys* 1, 21, 1536-1538, Doi 10.1143/Jap.21.1536, 1982.

135 Thieser, J., Schuster, G., Schuladen, J., Phillips, G. J., Reiffs, A., Parchatka, U., Pohler, D., Lelieveld, J., and Crowley, J. N.: A two-channel thermal dissociation cavity ring-down spectrometer for the detection of ambient NO₂, RO₂NO₂ and RONO₂, Atmos Meas Tech, 9, 553-576, 10.5194/amt-9-553-2016, 2016.

Wehry, E. L.: Modern fluorescence spectroscopy, Modern analytical chemistry, Plenum Press, New York, v. <1-4 > pp., 1976.

York, D., Evensen, N. M., Martinez, M. L., and Delgado, J. D.: Unified equations for the slope, intercept, and standard errors of the best straight line, Am J Phys, 72, 367-375, 10.1119/1.1632486, 2004.

Laser induced fluorescence based detection of atmospheric nitrogen dioxide and comparison of different techniques during the PARADE 2011 field campaign

5 Umar Javed^{1,2}, Dagmar Kubistin^{1,3,4}, Monica Martinez¹, Jan Pollmann¹, Markus Rudolf¹,
Uwe Parchatka¹, Andreas Reiffs¹, Jim Thieser¹, Gerhard Schuster¹, Martin Horbanski⁵, Denis Pöhler⁵,
John N. Crowley¹, Horst Fischer¹, Jos Lelieveld¹, and Hartwig Harder¹

¹Department of Atmospheric Chemistry, Max Planck Institute for Chemistry, Mainz, Germany

²Institute of Energy and Climate Research, IEK-8: Troposphere, Forschungszentrum Jülich GmbH, Jülich, Germany

10 ³University of Wollongong, School of Chemistry, Wollongong, NSW, Australia

⁴German Meteorological Service, Meteorological Observatory Hohenpeissenberg (MOHp), Hohenpeissenberg, Germany

⁵Institute of Environmental Physics, University of Heidelberg, Heidelberg, Germany

15 *Correspondence to:* Hartwig Harder (hartwig.harder@mpic.de) or Umar Javed (u.javed@fz-juelich.de)

Abstract. GANDALF (Gas Analyzer for Nitrogen Dioxide Applying Laser-induced Fluorescence), a new instrument for the detection of nitrogen dioxide based on the laser-induced fluorescence (LIF) technique, is presented in this paper. GANDALF is designed for ground based and air-borne deployment with a robust calibration system. In the current setup, it uses a multi-mode diode laser (447 – 450 nm) and performs in situ, continuous, and autonomous measurements with a laser pulse repetition rate of 20 5 MHz. The performance of GANDALF was tested during **the summer of year 2011 (15 Aug.-10 Sep.)** in a field experiment at **Kleiner Feldberg, Germany**. **The location** is **within** a forested **region** with urban influence where NO_x levels were between 0.12 and 22 parts per billion by volume (ppb). Based on the field results, the limit of detection is estimated at 5 – 10 parts per trillion by volume (ppt) in 60 s at a signal to noise ratio (SNR) of 2. The overall accuracy and precision of the instrument are better than 25 5 % (1 σ) and 0.5 % + 3 ppt (1 σ min⁻¹), respectively. A comparison of nitrogen dioxide measurements based on several techniques during the field campaign PARADE-2011 is presented to explore methodic differences.

1 Introduction

Tropospheric nitric oxide (NO) and nitrogen dioxide (NO₂) are key species in atmospheric chemistry and are strongly coupled due to their fast photochemical interconversion generally combined as NO_x (= NO + NO₂). Nitrogen oxides act as key catalyst in 30 the formation of tropospheric ozone (O₃) (Crutzen, 1979). NO_x also plays an important role in the oxidation capacity of the troposphere by affecting the abundances of O₃, hydroxyl radical (OH), and nitrate radical (NO₃).

The main sources of NO_x in the troposphere are combustion processes, predominantly fossil fuel use, biomass burning, microbial production in soils, transport from the stratosphere and lightning, the latter two directly affecting the free troposphere [e.g. (Logan, 1983)] **along with aircraft emissions (Strand and Hov, 1996)**. NO_x emissions from the surface are mostly in the 35 form of NO which is converted to NO₂ by the reaction of NO with O₃, the hydroperoxyl radical (HO₂), organic peroxy radicals (RO₂), and halogen oxides. The oxidation of nitrogen oxides in the atmosphere leads to the formation of several reactive nitrogen species, some of which act as reservoirs for NO_x, denoted by NO_z¹. The NO_x lifetime is largely determined by its oxidation into nitric acid (HNO₃) by OH during daytime, and in polluted air also by the heterogeneous loss of N₂O₅ (formed by NO₂+NO₃) on

¹ NO_z = NO₃ + 2N₂O₅ + HNO₃ + HONO + RO₂NO₂ + RONO₂ + HNO₄ + Particulate Nitrate + ...

wet surfaces during the night, e.g. on aerosols and cloud droplets. The tropospheric lifetime of NO_x is in the range of hours to
40 days and it is generally shorter closer to the surface of Earth compared to high altitudes [e.g. (Ehhalt et al., 1992)]. Because of its
relatively short lifetime, the transport distance of NO_x is limited, compared to other primary pollutants like carbon monoxide
(CO) and methane (CH_4) that disperse on hemispheric and global scales.

The wet and dry deposition of HNO_3 is considered the major sink for NO_x . Uncertainties in the NO_x budget have
recently been highlighted (Stavrakou et al., 2013). These include the uncertainty in the estimate of the rate coefficient for
45 $\text{NO}_2 + \text{OH}$ under tropospheric conditions (Mollner et al., 2010), a lack of proper representation in chemical mechanisms for the
loss of NO_x via organic nitrate formation (Browne and Cohen, 2012), and the formation of HNO_3 in a minor branch of the
reaction between NO and HO_2 (Butkovskaya et al., 2007) which showed significant impacts on the concentration of NO_x , OH,
 HNO_3 and related chemistry (Cariolle et al., 2008;Gottschaldt et al., 2013). Additionally, a lack of agreement between modelled
and measured OH concentrations over forests (Lelieveld et al., 2008;Kubistin et al., 2010) and urban regions (Hofzumahaus et
50 al., 2009) contribute to uncertainty about NO_x chemistry. In summary, NO_x even in the low ppt range is important for
understanding the tropospheric O_3 production (Lelieveld and Crutzen, 1990;Carpenter et al., 1997) and the cycling of radicals
(Monks, 2005). Therefore, it is of great importance to have accurate NO_x measurements from regional to global scales.

Tropospheric mixing ratios of NO_x can vary from a few ppt to ~~400 hundreds of~~ ppb, depending on remote (Hosaynali
Beygi et al., 2011) and urban conditions (Clapp and Jenkin, 2001), respectively. The high temporal and spatial variability of NO_x
55 with the wide concentration ranges challenges its measurements. Briefly, several different methods have been used to measure
 NO_x in the atmosphere. ~~The Photofragmentation Two-Photon Laser-Induced Fluorescence (PF-TP-LIF) (Sandholm et al.,
1990;Bradshaw et al., 1999) and chemiluminescence (Fontijn et al., 1970) methods are well known for direct in situ NO
detection. In the past, an indirect detection of NO_2 with these techniques has been performed by converting $\text{NO}_2 \rightarrow \text{NO}$ via
photolytic/catalytic process followed by NO detection. However, in the case of NO_2 to NO conversion, a potential interference
from NO_2 species cannot be fully excluded for the NO_2 measurement, e.g. (Crawford et al., 1996;Villena et al., 2012;Reed et al.,
60 2016). ~~The Photofragmentation Two-Photon Laser-Induced Fluorescence (PF-TP-LIF) in situ method was used in the past
(Sandholm et al., 1990) to measure NO directly by using a spectroscopically selective laser to excite the molecule with
subsequent fluorescence detection (Bradshaw et al., 1999). An indirect detection of NO_2 with this technique is also possible by
converting $\text{NO}_2 \rightarrow \text{NO}$ via photofragmentation followed by NO detection. The $\text{NO}_2 \rightarrow \text{NO}$ photolytic conversion was performed
using a XeF excimer laser at 353 nm (Sandholm et al., 1990) or Nd:YAG laser at 355 nm (Bradshaw et al., 1999). Whilst the PF-
TP-LIF technique is adequate for an in principle interference free detection of NO, the indirect detection of the NO_2 suffers from
interferences originating especially from nitrogen containing species [e.g. (Crawford et al., 1996)]. The most common in situ
method to measure NO_x is based on chemiluminescence detection. In this technique, the atmospheric NO reacts with an added
excess amount of O_3 to produce electronically excited NO_2 . The light intensity from the relaxation of electronically excited NO_2
70 is measured and proportional to the atmospheric NO (Fontijn et al., 1970). The chemiluminescence technique is arguably the best
method available to measure NO directly because of better cost effective maintenance. This instrument is often combined with
indirect NO_2 detection by converting it to NO. The $\text{NO}_2 \rightarrow \text{NO}$ conversion is either performed using a heated molybdenum
catalyst or photolytic conversion. However, in the case of NO_2 to NO conversion, a potential interference from NO_2 species
cannot be fully excluded for the NO_2 measurement, e.g. (Villena et al., 2012;Reed et al., 2016). Therefore, a direct detection of
75 NO_2 is advantageous. Techniques like cavity ring down absorption spectroscopy (Osthoff et al., 2006), tunable diode laser
absorption spectroscopy (Herndon et al., 2004), cavity enhanced absorption spectroscopy (Wojtas et al., 2007), **cavity-enhanced
differential optical absorption spectroscopy (Platt et al., 2009)**, and cavity attenuated phase shift spectroscopy (Ge et al., 2013)
provide direct in situ detection of NO_2 . Another promising method for a direct NO_2 detection is based on the laser-induced~~~~

80 fluorescence technique. The LIF method for NO₂ provides highly selective and sensitive measurements and it has already been demonstrated successfully in the past with detection limits reaching down to about 5 ppt min⁻¹ (Thornton et al., 2000; Matsumoto and Kajii, 2003).

85 An overview of LIF NO₂ systems from the literature is given in Table 1. LIF systems have been used for many years but the detection limits are sometimes not suitable for detection in a remote region, especially in some of the earlier attempts (George and O'Brien, 1991; Fong and Brune, 1997; Matsumoto et al., 2001; Taketani et al., 2007). In the last decade, owing to the advancements in lasers, better detection limits have been achieved. The LIF systems have shown good selectivity and sensitivity (Thornton et al., 2000; Matsumi et al., 2001; Matsumoto and Kajii, 2003; Dari-Salisburgo et al., 2009; Di Carlo et al., 2013), but most of these systems have large (typically > 50 kg) and complex laser systems. The availability of much smaller and lighter diode lasers have made it possible to build compact instruments with the caveat of lower laser power and higher detection limits. Here for GANDALF, a high power, lightweight diode laser (< 2 kg) system is used to achieve a compact design with detection 90 limits comparable to those of the best performing larger instruments.

In the following the newly developed LIF instrument for the direct NO₂ detection is described. Results from the first field deployment in a semi-rural region are reported to demonstrate the performance of the instrument. Measurements of trace gases along with meteorological parameters were carried out during the campaign, including NO₂ measurements based on several techniques, namely LIF, cavity ring down absorption spectroscopy, two-channel chemiluminescence detection, cavity-enhanced differential optical absorption spectroscopy, and long-path differential optical absorption spectroscopy. Being the first 95 deployment of GANDALF, this opportunity provided the means for a detailed comparison to other methods under real atmospheric conditions.

2 The instrument description

100 2.1 The operational method

The measurements of GANDALF are based on laser-induced fluorescence at low pressure (<10 hPa). The NO₂ molecule is excited by a diode-laser with a wavelength well above the photolysis threshold ($\lambda > 420$ nm for NO₂) and the red-shifted fluorescence is detected during laser-off periods.



110 The NO₂ fluorescence has a broad spectrum. It starts at the excitation wavelength and extends into the infra-red region (Wehry, 1976). But still, the major fraction of the fluorescence still lies in the visible region (Sakurai and Broida, 1969; Sugimoto et al., 1982). The detected fluorescence $h\nu'$ is directly proportional to the amount of NO₂ in the cell. The background signal due to scattering and dark counts of the detector is determined by frequently measuring zero air (zero-NO₂). The atmospheric mixing ratios of NO₂ are derived by using Eq. 1.

$$\text{NO}_2 = \left[\frac{\text{Signal} - S_{BG}}{\alpha_c} \right] \quad \text{Eq. 1}$$

Where ‘Signal’ is in counts s^{-1} and α_c is the calibration factor or sensitivity in counts $s^{-1} \text{ppb}^{-1}$. α_c is derived from the slope of counts versus known amounts of NO_2 . ‘ S_{BG} ’ is the background signal in counts s^{-1} . The quality of zero air is further discussed in section 3.

The mechanical and optical parts of the LIF detection axis are presented schematically in Fig. 1. All mechanical parts inside GANDALF are black anodised and most optical components are continuously flush with zero air ($3 \times 50 \text{ sccm}$) (Fig. 1, no.1) during the period of operation to avoid dead air pockets, fog, dust, etc. The inlet for the sampling flow **line** is a small orifice with a diameter of 0.7 mm (Fig. 1, no.2). The distance from the point of entrance at the orifice to the centre of the detection cell is about 150 mm. This combination of orifice size and scroll pump provides a pressure of 7 hPa inside the detection cell, with a sampling flow of about 4100 sccm. The time required for air molecules from the point of entrance to reach the centre of the detection cell is less than 30 ms. The **diode laser**² (Fig. 1, no.3) in this system has a maximum output power of 250 mW with an on-off modulation frequency of 5 MHz. The wavelength (λ) of the diode laser is in the range of 447 \rightarrow 450 nm. The convolution of the laser profile and the NO_2 absorption cross-section (Vandaele et al., 2002) yields an effective NO_2 absorption cross-section of $5.3 \times 10^{-19} \text{ cm}^2 \text{ molecule}^{-1}$. The laser beam is directed into the detection cell by using motorised mirrors (Fig. 1, no.5). These mirrors are coated to achieve high reflectivity (99.8 %) for a light incidence at 45° with a wavelength of 450 nm. A **Herriot cell** (Herriott et al., 1964) is used to produce multiple passes to enhance the laser light, and focus at the centre of the detection cell. The detection cell of GANDALF is positioned between the Herriott cell mirrors (Fig. 1, no.5), which have approximately 99.99 % reflectivity (IBS coating)³ in the spectral range of 445 nm to 455 nm. The distance between the mirrors is twice their radius of curvature ($R = 128 \text{ mm}$). Any fluorescent contaminants from the mirrors are measured as a part of the background signal. The multi-passed laser beam encompass a circle of about 8 - 10 mm diameter at the centre of the detection cell. A **photon counting head**⁴ (PMT) is used for the fluorescence detection. The PMT is located in a tube (Fig. 1, no.6) perpendicular to the sampling flow line. The effective sensor area of the PMT is 5 mm in diameter and has a GaAsP / GaAs photocathode⁵. The PMT is sensitive to wavelengths between 380 nm and 890 nm, with peak sensitivity at 800 nm with a maximum quantum efficiency of 12 %. The fluorescence signal is focused onto the PMT by collimating lenses (Fig. 1, no. 7). An aluminium concave mirror (Fig. 1, no.8) located opposite of the PMT redirects additional fluorescence photons towards the detector. In front of the PMT, **interference filters**⁶ (Fig. 1, no.9) are used to remove contributions of light scattered from the walls of the sampling chamber, as well as from Rayleigh and Raman scattering. The filters have the cut-off wavelength (block radiation below this wavelength) of 470 nm and 550 nm respectively, with an average transmission of 98 % in the spectral range from cut-off wavelength + 3 nm to 900 nm. The reflectivity of the filters is higher than 99.7 % for the spectral ranges of about 8 nm below the cut-off wavelengths. The filters have a very small ($< < 1 \%$) absorption for almost the entire spectral regimes. However on the edge of the photonic stop band (cut-off wavelength) the absorption can be up to 7 % and 4 % for the filters with cut-off wavelength of 470 nm and 550 nm, respectively. At this position, the photon density reaches to its maximum which increases the probability of absorption of a photon. If this absorption at about the cut-off wavelength exist than this can potentially amplify the luminescence. The fluorescence contamination is corrected using the background signal measurements. An optical system (Fig. 1, no.10) based on photodiodes and a NO_2 filled cuvette is installed to monitor the change

² Omicron Lasertechnik (CW Diode-Laser), laserprodukte GmbH, Germany

Power stability $< 1 \%$ hour⁻¹, pointing stability: $< 10 \mu\text{rad}$

Beam diameter: 2.55 (perpendicular: $0^\circ/\text{mm}$) & 2.53 (parallel: $90^\circ/\text{mm}$)

³ ATFilms (IBS coating), USA

⁴ Hamamatsu (H7421-50), Japan, Count sensitivity: $2.1 \times 10^5 \text{ s}^{-1} \text{pW}^{-1}$ at 550 nm and $3.9 \times 10^5 \text{ s}^{-1} \text{pW}^{-1}$ at 800 nm

⁵ Radiant sensitivity of 87.4 mA W^{-1}

⁶ Barr Associates, Inc., USA

150 in the wavelength and power of the diode laser. The stray light in the system is reduced to a minimum by using a combination of baffles. There are different types of baffles (Fig. 1, no.11 and 12) used in the system to reduce scatter from walls or mirrors. The shape of a baffle surface is based on a zigzag pattern with a 30° angle. The sharpened edges of a baffle provide less surface area for the laser light to scatter and have the characteristics of a light trap. ~~The surface of the diode laser and PMT are continuously kept at a constant temperature by a circulated water (20°C or 25°C avoiding condensation) chiller.~~

155 The diode laser has a ‘Deepstar’ mode, which is used as an advantage for the system. While operating in this mode with the repetition rate of 5 MHz, there is no laser radiation during the off period and the NO₂ fluorescence is detected during the laser off period. To determine the optimum sensitivity as a function of the repetition range, the relative NO₂ fluorescence intensities for different on-off cycles has been calculated by taking into account key parameters like NO₂ absorption cross-section, pressure, flow velocity, fluorescence lifetime, and the power of the diode laser. The calculated sensitivity for different laser on-durations is shown in Fig. 2 (Left-side) based on 1 ppb of NO₂ as a function of off-period duration. For a comparison to current operational on-off cycles, three different on-periods are shown in Fig. 2 (Left-side). The best sensitivity of the instrument is achievable by operating the diode laser at 5 MHz, 100 ns on, 100 ns off.

165 A counter card is used for the data acquisition. There is no need for synchronisation as the counter card itself triggers the laser pulse. The timing system is entirely controlled by an FPGA (field-programmable gate array), utilizing an external crystal oscillator of 20MHz nominal frequency with a stability of +/-2.5ppm over the temperature range of -30°C to +75°C. All internal frequencies are derived from this clock by means of a PLL (phase-locked loop) in the FPGA. The triggering occurs at a fixed rate of 5 Mhz. The delay caused by the length of the trigger cable (propagation delay of the pulse), the laser power supply unit, propagation delays from detector to FPGA, etc. is compensated with a programmable delay for the data acquisition in the FPGA. So the FPGA logic recognises when it should start recording the data after it emitted the trigger pulse and waits the specified amount of programmed clock cycles after emitting the trigger. The time-resolved raw signal (both on-off cycle) are stored in 4 ns bins (4 ns bin = 1 channel) for a specified time of integration (typically 1 s). For the total fluorescence signal 20 of these channels are summed up and used as a signal for NO₂. The first 5 channels or 20 ns of the laser off period are ignored because these channels still contain some scattered light signals from the laser light and walls of detection cell [Fig. 2 (Right-side)].

170 The surface temperature of the PMT and laser is kept at a temperature of 20°C or 25°C (avoiding condensation) by circulating water. This provides the heat sink for the internal thermoelectric cooling of the PMT (@ 0°C) and laser (@ 25°C). The internal cooling is the default setting from the manufacturer. The internal temperature cannot be regulated by an external cooling. The external temperature should be in the range of 5-35°C along a sufficient heat exchange system (fan cooling, water circulation etc.). Moreover, the dark counts on the PMT signal are in the order of < 50 counts s⁻¹ for the channels used for the NO₂ fluorescence detection. The major reason for the background signal, larger than the dark signal typically by a factor >25, is expected to be fluorescence contamination from the Herriot cell mirrors existing in the red region of wavelength. For a stable (parameters like power, wavelength, shape of the beam etc.) laser operation, an external temperature range is within 15-30°C. This range is sufficient to keep the internal temperature of the laser at 25°C. A laser operation out of the specified range would lead to shut-off/potentially damage the laser.

185

2.2 Calibration system

The LIF method is not an absolute technique and requires calibration. The sensitivity (Eq. 1) of GANDALF depends on e.g. background noise, laser power or wavelength, temperature, pressure, residence time in the sampling line, etc. It is determined

using NO₂ concentrations generated by gas phase titration of NO to NO₂ by means of O₃ (R. 3) similar to the one described by e.g., (Ryerson et al., 2000). Using commercial available NO₂ gas cylinders at low concentrations (Thornton et al., 2000; Dari-Salisburgo et al., 2009), was not chosen due to its open questions with its long term stability at low concentration. The calibration system is described in the following sections.

The NO calibration mixture for the gas phase titration is traceable to a primary NIST⁷ standard (4.91 ± 0.04 μmol mol⁻¹ in nitrogen). The overall uncertainty of the NO calibration mixture is 2 %. NO is almost completely (> 98 %) consumed during gas phase titration with O₃ in the calibrator. This is achieved by using a high concentration (> 1.4 ppm) of O₃. NO₂ also reacts with O₃ to form NO₃ (R. 4). The reaction of NO₂ with O₃ (R. 4) is slower by 3 orders of magnitude compared to the reaction of NO with O₃ (R. 3), with a reaction rate of 3.5 × 10⁻¹⁷ cm³ molec⁻¹ s⁻¹ compared to 1.8 × 10⁻¹⁴ cm³ molec⁻¹ s⁻¹ at 298 K (Atkinson et al., 2004), respectively. However, at higher concentrations and due to the long residence times, the reaction between NO₂ and O₃ can become important, leading to a loss of NO₂ generated in the calibrator with subsequent losses due to further reaction between NO₂ and NO₃ (R. 5).



Numerical simulations are used to assess the optimum setup for the calibration device by studying the impact of different parameters like concentrations levels, residence time, flow rates, pressure, etc. Based on box model (BM) simulations and verified by lab experiments, a PFA (Perfluoroalkoxy) reaction chamber for the completion of the gas phase titration between NO and O₃ has been designed to achieve maximum conversion efficiency for NO → NO₂. The BM simulation is shown in Fig. 3 for typical calibration parameters⁸. The mixing ratios of NO, O₃, and NO₂ are plotted as a function of residence time in the left panel of Fig. 3. This simulation predicts that more than 99 % of NO is converted to NO₂ within the residence time of 7.5 s inside the reaction chamber. The formation of NO₃ and N₂O₅ in the reaction chamber is negligible (< 0.5 ppb) compared to NO₂ (> 100 ppb). The formation of NO₃ and N₂O₅ can thus only raise < 1 % uncertainty in the generated NO₂ for typical operating conditions of the calibrator. After the reaction chamber, the calibration gas mixture is further diluted with zero air to achieve a required range (close to ambient levels) of NO₂ mixing ratios.

The calibration system was tested for different concentrations of O₃. Figure 4 shows the NO₂ signal of the PMT (after dilution of the calibration gas) based on different O₃ mixing ratios in the reaction chamber for a constant NO concentration (about 0.1 ppm). For O₃ concentrations below 1 ppm non stoichiometric conversion of NO was observed as expected. The PMT signal reached a maximum at about 1.356 ppm and this signal is explained by the derived NO₂ concentration from the BM simulation. The decrease of the PMT signals at higher O₃ concentrations above 1.4 ppm mainly due to loss of NO₂ in reactions R. 4 and R. 5. The amount of NO₂ generated in the 'NO + O₃' titration is much less sensitive to O₃ than to NO as losses of NO₂

⁷ National Institute of Standards and Technology, USA

⁸ For this specific simulation, initial parameters;

NO = 5 sccm × 10.55 ppm,

O₃ = 500 sccm × 1.7 ppm,

residence time in the reaction chamber = 7.5s,

flow = 8000 sccm

temperature and pressure = 298 K and 1013.25 hPa

(R. 4) also being dependent on O₃ for the chosen parameters. If O₃ is increased by 1 ppm above the optimum mixing ratio of 1.3 ppm (Fig. 4), NO₂ is reduced by only 1 %. The O₃ concentrations are always kept above this threshold limit and the concentrations are measured using an O₃ analyser⁹ with a typical precision of 5 %. Above the threshold, a 5 % change in O₃ produces an uncertainty in NO₂ of less than 0.5 %.

A NO_x analyser¹⁰ was used to determine the remaining concentrations of NO inside the calibrator after the gas phase titration. About 99 % of NO is consumed in the gas phase titration for most of the cases at O₃ > 1.4 ppm. There are two different regimes in the calibration system based on different NO and O₃ concentrations and different flow rates: (1) gas phase titration in the reaction chamber and (2) dilution with zero air after the reaction chamber. Considering the flow rates and dimensions of the gas lines, the theoretically calculated total residence time based on the plug flow assumption is 7.73 s. While the total residence time for the calibration gas in the calibration system is also determined experimentally by using Eq. 3.

$$NO_{GPT} = D[NO_i](e^{-k_{R,3}[O_3]t_1})(e^{-k_{R,3}[O_3]Dt_2}) \quad \text{Eq. 2}$$

$$\Rightarrow [t_1 + Dt_2] = - \left[\frac{\ln\left(\frac{NO_{GPT}}{D[NO_i]}\right)}{k_{R,3}[O_3]} \right] \quad \text{Eq. 3}$$

In Eq. 3, 'NO_{GPT}' is measured with the NO_x analyser and is defined as the NO concentration remaining in the calibration gas after the gas phase titration and dilution. [NO_i] is the initial concentration of NO before the gas phase titration. 'D' is the dilution factor after the reaction chamber. 't₁' is the residence time for the reaction chamber and 't₂' is the dilution dependent travel time for a NO₂ molecule from the exit of the reaction chamber to the inlet of GANDALF. [O₃] in Eq. 3 is the concentration in the reaction chamber. 'k_{R,3}' is the temperature dependent rate coefficient for R. 3. There are two slightly different (< 6% based on rate constant at 298K) values reported in the literature for the temperature dependent k_{R,3} as follows:

$$k_{R,3} = 3 \times 10^{-12} \times e^{\left(\frac{-1500}{T}\right)} \quad (1.9 \times 10^{-14} \text{ cm}^3 \text{ molec}^{-1} \text{ s}^{-1} \text{ at } 298\text{K}) \quad (\text{Sander et al., 2011})$$

$$k_{R,3} = 1.4 \times 10^{-12} \times e^{\left(\frac{-1310}{T}\right)} \quad (1.8 \times 10^{-14} \text{ cm}^3 \text{ molec}^{-1} \text{ s}^{-1} \text{ at } 298\text{K}) \quad (\text{Atkinson et al., 2004})$$

Based on Eq. 3, the average value of total residence time [t₁ + D t₂] is 7.32 s ± 0.25 s (Sander et al., 2011) or 8.38 s ± 0.29 s (Atkinson et al., 2004) as shown in Fig. 5. The estimated accuracy of these two values for the total residence time is 6.5 % (1σ).

The temperature and pressure also affect the formation of NO₂ inside the reaction chamber, and these effects were tested with the box model. In the simulations all parameters except temperature or pressure are kept constant. At a lower temperature the reaction between NO and O₃ slows down leading to changes in the conversion efficiency from NO to NO₂. This can potentially lead to a change in the conversion efficiency from NO to NO₂. In our case, many electrical parts (electronic valves, ozone generator, and mass flow controllers) are installed inside the calibration unit. In a fully operational mode for one day, the temperature build up in the calibration unit is 8-10°C higher than ambient temperatures. From our experience/observations, conditions with a temperature lower than 20°C inside the calibrator do not occur. According to the box model simulations temperature variations within 5 - 45 °C leads to an overall relative uncertainty of 1 % (1σ) for the whole range. Similarly, the

⁹ ANSYCO, O3-41M, 'Analytische Systeme und Componenten GmbH', Germany

¹⁰ Model: ECO PHYSICS CLD 780 TR, Switzerland

260 impact on the calibration gas due to a change in the atmospheric pressure is not significant. Based on the box model simulations, the relative uncertainty in the NO₂ concentration of calibration gas due to a change in the atmospheric pressure over an interval of 800 – 1013 hPa is below 0.5 % (1σ).

265 The calibration gas for GANDALF primarily contains N₂ (~79.5 %) and O₂ (~20.5 %) with H₂O vapour (< 25 ppm). The level of H₂O vapour in the atmosphere can reach up to about 3 % (Seinfeld and Pandis, 2006). The sensitivity of the instrument is reduced by atmospheric H₂O vapour because collisions with H₂O molecules quench the NO₂ fluorescence. The H₂O dependency is evaluated experimentally by diluting the calibration gas with known amounts of water vapour concentrations and its effect on sensitivity during field measurements is corrected by using simultaneous measurement of H₂O vapour in the atmosphere. The H₂O concentrations during calibration are determined using an existing calibration system for the LIF-OH instrument (Martinez et al., 2010). The decrease (relative to < 25 ppm of water vapour) in the sensitivity for GANDALF is 270 5 % ± 1 % (1σ) at 1 % of atmospheric H₂O vapour.

A robust calibration system has been developed for the automated calibration of the instrument. GANDALF is frequently calibrated (up to 8 times in 24h) during field operations to track changes in sensitivity. **Generally, some factors can contribute to a change in the sensitivity e.g., stability of the optics alignment, cleanness of the optics, temperature related effect of electronics, stability of the calibration signal etc.** An example for a calibration plot is shown in Fig. 6. The calibration system is controlled by Mass Flow Controllers (MFC)¹¹ and electronic valves¹². All MFC are calibrated using a DryCal¹³ sensor which is traceable to a NIST standard (NIST traceability is confirmed by Westphal¹⁴). The uncertainty in the set flows, based on a certified value, is 1 % (level of confidence 95 %). O₃ is generated for the calibration using an ozone generator¹⁵. Different NO₂ mixing ratios are achieved by changing the NO flow (range up to 10 sccm), while the O₃ concentration (> 1.4 ppm) and flow (500 sccm) are kept constant. Figure 7 shows a schematic of the setup for the automated calibration procedure of GANDALF. A small pump (calibration pump) is connected to the main sampling line of GANDALF. A three-way electronic valve (EV2) and a manual needle valve (MNV) are attached in front of the calibration pump. To minimise any line effects such as a decomposition of species like PAN, the chemical reaction of the ambient NO and O₃, etc., the residence time in the sampling line is kept at less than 0.1 s by a flow ≥ 10000 sccm required during ambient air measurements. GANDALF has a flow of 4100 sccm through the pin hole and the rest of the flow is diverted to the main exhaust by the calibration pump. The amount of total sampling flow can be increased or decreased by adjusting the manual valve MNV. 280 285

During ambient air measurements, valve EV2 is opened for line L1 **at the position P1** (Fig. 7) and allows an extra flow of about 8000 - 9000 sccm to pass from the sampling flow to the calibration pump (~~direction shown by the white arrow in Fig. 7~~). Line L1 is simultaneously used to condition the NO calibration line with a flow of 2 sccm NO gas, which goes directly to the exhaust without entering ~~the sampling line measurement cell~~. **The direction for the conditioning flow along the bypass flow is shown by the green arrow in Fig. 7.** 290

Frequent zero-air measurements are necessary to monitor changes in the background signal of GANDALF. A ~~four-three~~-way electronic valve (EV3) and a mass flow controller (MFC Zero) are used to switch the zero air background flow (8000 sccm) on and off in the line L3 (**position P1 at EV3 in Fig. 7**). During background signal measurements, an excess of zero-air about 3900 sccm (blue arrow in Fig. 7) is diverted to the calibration pump through line L1 by setting the valve EV2 to position P1, along with about 5100 sccm flow of ambient air. 295

¹¹ MKS Instruments and Bronkhorst HIGH-TECH B.V, USA

¹² Solenoid Operated Diaphragm, Galtek, USA

¹³ DC-2, BIOS International Corporation, USA

¹⁴ WESTPHAL measurement and control technique GmbH & Co. KG, Germany

¹⁵ SOG2, 185nm, UVP - Ultraviolet Products, USA

During calibration the zero air flow is switched on (position P2 at EV3 in Fig. 7) and used for dilution of the calibration gas. Line ~~L1 is closed and instead line~~ L2 is opened by valve EV2 (position P2 at EV2 in Fig. 7) to remove the calibration gas overflow of 3900 sccm together with 5100 sccm from the ambient (illustrated by the red arrows in Fig. 7). For the gas phase titration, the flow of O₃ is switched on and off by the two-way electronic valve EV1 and MFC (O₃). ~~The O₃ analyser is used to check the concentration of O₃ produced by the ozone generator.~~ The flow of NO (1 - 10 sccm) is controlled by a mass flow controller [MFC (NO) in Fig. 7]. Since all overflows are diverted to an exhaust, this setup allows frequent checks of the GANDALF sensitivity and background signal without disturbing the ambient conditions for a nearby operating instrument. Based on calibrations during PARADE-2011, the repeatability of the sensitivity was 2.7 % (1 σ), with an overall uncertainty of the calibration system of approx. 5 % (1 σ).

2.3 Precision and limit of detection

~~The precision of the instrument was evaluated by using a set of randomly chosen individual calibrations from the field experiment (PARADE-2011). The relative precision of GANDALF for these calibrations is shown in Fig. 8. The relative precision on the randomly selected calibration data points was better than 0.5 % (1 σ at 1 min integration time) for most of the data points despite a few outliers (Fig. 8). For an overall precision of GANDALF, an absolute value of < 5 ppt, (1 σ) has to be added to the relative precision. This absolute value arises from the variability in the zero air signal and is derived from the intercept of a fit of absolute precisions of calibration points during PARADE versus mixing ratios of NO₂. The variations in background signal for GANDALF is proportional to the square root of the integration time. These variations around an average background signal measured with zero air dominate the precision of the instrument close to the detection limit.~~

The precision of the instrument was evaluated using a set of randomly chosen PMT signal (in s⁻¹ time resolution) during calibration periods from the field experiment (PARADE-2011). The relative precision was calculated based on the standard deviation of the PMT NO₂-signal for different NO₂ concentrations. The relative precision of GANDALF is shown in Fig. 8 as a function of NO₂ mixing ratios. It was better than 0.5 % (1 σ min⁻¹) for most of the dataset at >1ppb of NO₂. For an overall precision of GANDALF (especially at lower levels < 1ppb), an absolute value of about 3 ppt (1 σ) has to be added to the relative precision. This absolute value arises from the variations in the zero-air signal. The standard deviation of the PMT signals at different NO₂ concentrations can be extrapolated to zero for determination of the precision at background levels. It can also be calculated from the standard deviation of the zero-air signal. Both approaches give a similar result of about 3 ppt (1 σ) precision for our instrument.

The precision of the instrument background signal was also cross-checked using a continuous measurement of zero-air for about 50 minutes. In order to verify the square root dependency of the signal variability on integration time, an Allan deviation plot is used (Riley, 1995; Land et al., 2007). Figure 9 shows an overlapping (Riley, 2008) Allan deviation plot of variations in background signal versus averaging time. The variations in background signal with a 60 s integration time are equivalent to an absolute NO₂ value of about 3 ppt (1 σ). Figure 9 also shows that the random noise of the instrument background signal can be reduced by averaging, with a square root dependency on time, at least up to a 60 s period. The background signal of GANDALF is frequently checked during a field operation (e.g. during PARADE, 1 background signal measurement per hour).

The limit of detection (LOD) can be derived from the variation of the background signals. Based on the Allan deviation plot in Fig. 9, a limit of detection of about 3 ppt(1 σ) NO₂ for one minute averaged measurements is expected. The stated (Table 1) LOD of GANDALF was calculated using Eq. 4 (Taketani et al., 2007) at a signal-to-noise ratio SNR of 2 and considering the two times higher background signal.

$$LOD = \frac{SNR}{\alpha_c} \sqrt{\frac{2 \times S_{BG}}{t}} \quad \text{Eq. 4}$$

Where α_c is the calibration factor or sensitivity in counts ($s^{-1} \text{ ppb}^{-1}$), S_{BG} is the background signal in counts (s^{-1}) and t is the averaging time in seconds. The LOD for GANDALF, based on sensitivity and background measurements during the field experiment (PARADE-2011), varied between 5 and 10 ppt.

2.3 Interferences by other species

Several atmospheric gas species can absorb the 449 nm laser light inside the detection cell. This can lead to interference for the NO_2 measurements with GANDALF directly (photodissociation process) or indirectly (fluorescence).

Iodine monoxide (IO) has an absorption cross-section of $3.9 \times 10^{-18} \text{ cm}^2 \text{ molecule}^{-1}$ (Harwood et al., 1997) and is about a factor 8 larger than the NO_2 absorption cross-section at 449 nm. Even a few ppt of IO in the atmosphere can produce a significant fluorescence signal, especially in the marine atmosphere for which IO is mostly reported (Commane et al., 2011). The fluorescence lifetime of IO is only 1-10 ns (Bekooy et al., 1983; Newman et al., 1998). As described earlier, the initial 20 ns fluorescence signal is ignored in the GANDALF data evaluation. So the IO fluorescence signal after 20 ns becomes too small to significantly interfere with the NO_2 fluorescence signal.

Nitrogen containing inorganic species (NO_3 , N_2O_5 , HONO_2 , HO_2NO_2 , PAN, ClONO , ClNO_2 , and ClONO_2) can produce NO_2 by photodissociation which can happen inside the detection cell. N_2O_5 (Harwood et al., 1993), HONO_2 (Burkholder et al., 1993), HO_2NO_2 (Singer et al., 1989), PAN (Talukdar et al., 1995), and ClONO (Molina and Molina, 1977) are not known to photo-dissociate at this wavelength. The absorption cross-sections for ClONO_2 (Molina and Molina, 1979) and ClNO_2 (Ghosh et al., 2012) are smaller by about 4 orders of magnitude compared to that of NO_2 at 449 nm. The tropospheric concentrations of ClONO_2 and ClNO_2 are generally smaller to similar compared to ambient NO_2 . Hence, an interference from these species is highly unlikely.

NO_3 has a larger absorption cross-section (Wayne et al., 1991) at 449 nm compared to the previously described nitrogen-containing species. The effective absorption cross-section, calculated from (Wayne et al., 1991), is about a factor of 2 smaller than that of NO_2 at the wavelength of the diode laser. The recommended quantum yield for the photodissociation of NO_3 to $\text{NO}_2 + \text{O}$ is about 1 at wavelengths below 585 nm (Sander et al., 2011); hence, its fluorescence (Wood et al 2003) is insignificant compared to its photodissociation to NO_2 . Interference from photodissociation of NO_3 is therefore a two-photon process:



The lifetime of NO_3 can be estimated from Eq. 5.

$$\tau(\text{NO}_3) \approx \int \sigma_{\text{NO}_3}(\lambda, T) \times \phi_{\text{NO}_3}(\lambda, T) \times F(\lambda, T) d\lambda \quad \text{Eq. 5}$$

Where $\sigma(\lambda, T)$ is the effective absorption cross-section of NO_3 which is $2.7 \times 10^{-19} \text{ cm}^2 \text{ molecule}^{-1}$; $\phi(\lambda, T)$ is the quantum yield for NO_3 , and $F(\lambda, t)$ is the photon flux from the diode laser of about $10^{20} \text{ photons cm}^{-2} \text{ s}^{-1}$. The residence time of sampling air in

the effective beam area of the laser is much smaller (<0.001 s) compared to the NO_3 photodissociation lifetime (> 0.01 s). Due to this reason, any chance of a significant interference from the NO_3 photodissociation is highly unlikely. Moreover, the ratio of the atmospheric concentration between NO_2 and NO_3 is very high, e.g. during PARADE the median ratio $\text{NO}_2 / \text{NO}_3$ was 430 for $\text{NO}_3 > 0$ with a minimum value of 12.

Alkenes and aromatics (aldehydes and benzene) are also abundant in the troposphere. However, absorption of alkenes and aromatics occurs in the UV range (< 300 nm) (Keller-Rudek et al., 2013), well below the wavelengths used in GANDALF. Some carbonyls like glyoxal (CHOCHO), and methylglyoxal (CH_3COCOH) also have absorption in the blue region of the visible spectrum. The absorption cross-section values of CHOCHO , and CH_3COCOH are $5.28 \times 10^{-20} \text{ cm}^2 \text{ molecule}^{-1}$ (Horowitz et al., 2001), and $9.26 \times 10^{-20} \text{ cm}^2 \text{ molecule}^{-1}$ (Meller et al., 1991; Staffebach et al., 1995) at 449 nm, about a factor 10 and 5 smaller than the NO_2 absorption cross-section, respectively. Also the fluorescence from these species is not known to be present in the region of NO_2 fluorescence. So, the interference from these species is not important.

To minimise the impact (prior to the orifice) of heterogeneous or thermal conversion of species like PAN (*lifetime*¹⁶ ≈ 2327 s), HO_2NO_2 (*lifetime* ≈ 16 s), CH_3OONO_2 (*lifetime* ≈ 0.3 s), and N_2O_5 (*lifetime* ≈ 22 s) yielding NO_2 , a short residence time of < 0.1 s is generally used by keeping the sampling flow high, e.g. 12000 sccm in a 0.5 m long sampling line with a 4 mm internal diameter during PARADE-2011. After the orifice, the cell pressure is about 7 hPa and this would lead to increase even further the lifetime of above-specified species. Whereas the residence time after the orifice is less than 30 ms. So a chance of interference in the low-pressure region from the thermal conversion is highly unlikely. An intercomparison of GANDALF and other measurements of NO_2 during PARADE-2011 was conducted to look for systematic dependencies of the differences between the different measurements on several measured atmospheric quantities. No evidence for a potential interference has been found for GANDALF (Section 3.2).

3 Field Experiment: PARADE-2011

The PARADE, **P**articles and **R**adicals: **D**iel observations of the impact of urban and biogenic Emissions, field experiment took place at the Taunus Observatory on Kleiner Feldberg (825m ASL¹⁷⁴⁶; 50.22° N, 8.45° E) in Germany from the 15th of August (DOY¹⁸⁴⁷ = 226) to the 10th of September (DOY = 252) 2011. The general focus of PARADE was to characterise summertime biogenic emissions and photochemistry in a forested environment with anthropogenic influence. The observatory is located in the vicinity of the Taunus region at the hilltop of Kleiner Feldberg. A total area of 5 km radius around the observatory is dominated by coniferous, broad leaved and mixed forest. The measurement platform was located at the top of the observatory. The site is often affected by anthropogenically influenced air from nearby cities such as Frankfurt/Main (30 km SE), Wiesbaden (20 km SW), Mainz (25 km SSW), and some roads within 5 - 10 km, depending on the wind direction. The temperature during PARADE varied within a range of 5 - 28 °C with an overall average of 14.8°C. The temperature conditions during PARADE can be subdivided into two phases. The periods of DOY = 226 - 237 and DOY = 243 - 246 for PARADE were slightly warmer and the temperature mostly stayed above 15 °C, whereas during the other periods of DOY = 238 - 242 and DOY = 248 - 252 the temperature was below 15°C. The relative humidity (RH) had an overall average value of 77 % and variations within the interval of 37-100 %. There were several episodes of rain during PARADE. In the later part of the campaign, fog persisted in the

¹⁶ The *lifetime* is calculated from IUPAC rate coefficient (temperature = 298 K and pressure = 1 bar) for the sampling line before the orifice.

¹⁷⁴⁶ above sea level

¹⁸⁴⁷ DOY (Day of year 2011)

early morning hours. Air masses at the observatory arrived predominantly from the southwest (SW) to the northwest (NW) side of Kleiner Feldberg. Sampling lines for most of the trace gas monitoring instruments were located within a 5 m² area at the top of the platform. The platform was about 8 m above ground and the top of the platform was above the forest canopy. An overview of the instrumentation and conditions during PARADE can be found e.g. in (Phillips et al., 2012; Bonn et al., 2014). Note that all data sets for analysis are based on available 10-minute averages.

3.1 NO₂ inter-comparison during PARADE

NO₂ concentrations were measured with eight different instruments. Six out of eight instruments sampled at the top of the platform. The measurement techniques, uncertainties, time resolutions and LOD are summarised in Table 2 for the instruments located on the platform. The average ambient concentrations of NO₂ during PARADE were approx. 2 - 3 ppb with a range of approx. 0.13 ppb to 22 ppb. NO₂ instruments listed in Table 2 represent in situ measurement techniques with the exception of the LP-DOAS (Long Path Differential Optical Absorption Spectroscopy).

A median value (based on 10 minute averages) of the atmospheric NO₂ concentration is derived from the NO₂ measurements of all individual instruments at the platform including LP-DOAS. For a valid correlation between the derived median NO₂ and individual NO₂ measurements, only those values of the median NO₂ were selected for which simultaneous data for all NO₂ measurements were available. Figure 10 shows the correlation between individual NO₂ measurements and the derived median NO₂ concentrations. The total uncertainties of individual instruments are shown as error bars on the y-axis while horizontal bars represents the standard deviation of the derived median NO₂. The regression is done by using a 'bivariate' fit according to the method described in (York et al., 2004; Cantrell, 2008).

LP-DOAS: This instrument is based on traditional Differential Optical Absorption Spectroscopy (DOAS) (Platt et al., 1979; Perner and Platt, 1979), and follows the Beer-Lambert law. DOAS allows direct and absolute measurements of multiple trace gases in the atmosphere by using the distinct absorption band structure of the specific molecule (i.e. calibration is not needed) (Platt and Stutz, 2008). LP-DOAS is based on active remote sensing and requires an artificial light source (Pöhler et al., 2010). It provides an average concentration of NO₂ or other trace gases through quantitative detection using the absorption over a light path of typically a few kilometres. The instrument in this study is a well-established instrument and has been a part of many field campaigns (Pöhler et al., 2010). During PARADE, the optical path length was approximately 2.5 km and the light source as well as the spectrograph was located on the platform. The optical retro-reflector reflecting the light back to the telescope was located on the mountain Großer Feldberg (Distance = 1.23 km and Height = 37 m). Therefore the LP-DOAS measurement delivers values integrated along a 1.2 km straight line starting at the platform to the retro-reflector. The correlation ($R^2 = 0.96$) plot between LP-DOAS and the derived median NO₂ values is shown in subplot E of Fig. 10. The slope of the fit is 1.02 ± 0.005 with a negligible y-intercept of -0.002 ± 0.009 ppb and these values are within the uncertainty of the instrument. The uncertainty of LP-DOAS is mainly due to errors in the absorption cross-sections of NO₂. A larger scatter between the LP-DOAS to the in situ instruments is expected due to the sampling of different air masses (A1 in Fig. 11).

CE-DOAS: Cavity-Enhanced DOAS (Platt et al., 2009) measurements of NO₂ were also available during PARADE. This method is based on Differential Optical Absorption Spectroscopy (DOAS) combined with a cavity and provides in situ measurements of trace gases (Platt et al., 2009). CE-DOAS requires calibration of the absorption light path in the cavity. This was performed with the measurement of two different Rayleigh absorbers (Helium, and air) according to (Washenfelder et al., 2008). The campaign was also the first field trial for this instrument with a reported error of measurements in the range of 5 - 10 %, mainly due to the accuracy of the light path calibration. The CE-DOAS and the CRDS shared the same sampling line. The

slope and the y-intercept for CE-DOAS versus the median derived NO₂ is 0.92 ± 0.007 and -0.032 ± 0.01 ppb, respectively, with $R^2 = 1$ as shown in subplot [F] of Fig. 10. The difference to the median value is well within the range of instrumental uncertainty of this prototype. A further development of this prototype is the ICAD (iterative cavity enhanced DOAS) from Airyx GmbH.

CRDS: Besides the DOAS instruments, another NO₂ measurement technique using a Cavity Ring-Down Spectrometer (CRDS) was available (Thieser et al., 2016). CRDS is a cavity-assisted method like CE-DOAS (Platt et al., 2009). It is a direct method for in situ measurements which requires no calibration but only the background (zero-air) measurements. In CRDS, reflective mirrors are used across an optical cavity. To obtain the concentration of a trace gas with CRDS, absorption measurements to determine the time constant for exponential decay of the light intensity with and without an absorber are made in the optical cavity. During PARADE, the instrument inlet was located 2 m above the platform. An about 8 m long PFA tube was used for the sampling air. The slope and y-intercept in the case of CRDS are 1.06 ± 0.007 and 0.01 ± 0.01 ppb with correlation $R^2 = 0.99$ as shown in panel D of Fig. 10. The reported upper limit of uncertainty in the case of CRDS is $[6\% + 20 \text{ ppt} + (20 \text{ ppt} \times \text{RH}^{19+18}/100)]$ (Thieser et al., 2016). The differences between CRDS and the derived median NO₂ values are smaller than the instrument errors.

CLD/Blue-light converter (BLC): Along with the above mentioned absolute methods, the concentrations of NO₂ and NO were determined with a two-channel chemiluminescence detector (CLD). The instrument sampled air via ~8 m long PFA tubing at 2 m above the platform. The CLD instrument of MPIC is well-established, being an improved version (Hosaynali Beygi et al., 2011) of the ECO-Physics CLD 790 SR. In this instrument, NO₂ is detected by conversion via photolysis to NO, using a blue light converter at the wavelength of 395 nm, with subsequent detection of NO by chemiluminescence. The calibration of the system is done by using gas phase titration between NO and O₃ to produce stoichiometric quantities of NO₂. The correlation ($R^2 = 0.99$) between CLD and the derived median NO₂ values is shown in panel C of Fig. 10. Overall, the data of the CLD is about 5 % below the median, but this difference is within the uncertainty of the CLD measurement. The reported uncertainty of the CLD for the NO₂ measurements is 105 ppt or 10 % (Li et al., 2015). The slope and y-intercept are 0.95 ± 0.008 and -0.1 ± 0.01 ppb, respectively. A larger negative intercept could be related to measurements of higher background for the BLC unit (switch ON) leading to underestimation of ambient NO₂. An additional background signal is most likely due to decomposition of surface absorbed NO or NO₂ during the operational mode of the BLC unit (Teflon block).

GANDALF: The sampling flow rate (12000 sccm) provided a residence time of less than 0.1 s in a 0.5 m sampling line. This was sufficient to suppress the impact of heterogeneous or thermal conversion of NO₂ containing species to yield NO₂. The formation of NO₂ due to the reaction between ambient NO and O₃ in the sampling line was negligible. The campaign averages of the observed concentrations of NO, O₃ and NO₂ were 0.25 ppb, 44 ppb and 2.6 ppb respectively. Based on average NO and O₃ concentrations, the formation of NO₂ from the reaction 'NO + O₃' in the sampling line was less than 0.01 % with respect to the ambient NO₂ concentrations. Line loss or photolysis of NO₂ was avoided by using PTFE lines (Polytetrafluoroethylene) covered with a dark insulating material. The average pressure inside the detection cell for the entire period of PARADE was 6.95 ± 0.27 (1 σ) hPa. Several automated calibrations (2 - 8 per day) and background level measurements (once per hour) were conducted during PARADE to ensure the precision and accuracy of the instrument. Based on the hourly background level measurements, we established that the deviations for about 70 % (1 σ) of successive background signal measurements (no. of measurements > 500) were within an equivalent value of ± 8 ppt of NO₂. Any NO₂ impurity in the used zero air (hydrocarbon-free) would lead to under estimation of ambient NO₂ levels for PARADE and further contribute to the uncertainty. Nevertheless, previously describe deviations of 8 ppt in the background signal during PARADE could be a good indicator for this uncertainty.

¹⁹⁺¹⁸ Relative humidity in %

A malfunction of the O₃ generator occurred in the period 4 to 10 September that disturbed the GANDALF calibration system. Another indication that the NO₂ contamination in zero air used during PARADE-2011 was less than GANDALF's detection limit is that in the data analysis the y-intercept of other NO₂ in situ instruments (y-axis) vs GANDALF (x-axis) showed always a negative number. If the GANDALF zero-measurements would have significant NO₂ contamination the y-intercept should be positive (This figure is provided in the supplement). A correction of 12 % is introduced for the period 4 – 10 September, based on the correlation of GANDALF with the CRDS instrument prior to 4 September. During the last few days of this period, an extra baffle was installed in GANDALF. The baffle can be inserted easily into the detection block of GANDALF without disturbing the alignment of the laser. The advantage of the baffle is that it reduces the background counts by ~50 % while decreasing sensitivity by less than 5 %. The overall correlation between GANDALF and the derived median NO₂ is R² = 0.99 as shown in panel B of Fig. 10. The measurements of GANDALF tend to be 3 % higher compared to the derived median values of NO₂. This overestimation of slope from unity compared to the derived median value is within the range of the instrument uncertainties. The overall relative uncertainty of GANDALF during PARADE was about 5 % + 11 ppt and it showed an exponentially increasing trend from a higher to lower concentration of NO₂. This increasing trend is mainly driven by the error in the background measurements. The slope and y-intercept of the fit are 1.03 and 0.027 ppb with the absolute error of the fit being 0.006 and 0.01 ppb, respectively.

Generally, all instruments for NO₂ showed reasonable agreement with the derived median NO₂. Based on Fig. 10, GANDALF (+ 3 %), CRDS (+ 6 %) and LP-DOAS (+ 2 %) showed over-estimation compared to the derived median values while the data from CLD was about – 5 % and from CE-DOAS about – 8 % lower than the median values. The overall differences are within the experimental limitations and instrumental uncertainties. Results of the comparison between individual NO₂ measurements and the derived median NO₂ at different ranges of NO₂ mixing ratios are summarised in Table 3.

3.2 Ratio distribution of NO₂ measurements

Various measurements of trace gases, meteorological parameters, and photolysis frequencies during PARADE provided an opportunity to look for indications of systematic differences between NO₂ instruments. Ratios of the individual NO₂ measurements to GANDALF, which are referred to as “ratios” further in this section, are compared in respect of different atmospheric conditions. The distribution of ratios is shown as a histogram in the upper panel of Fig. 11 [A1, A2, A3, and A4] along their respective fits based on the normal distribution. The ‘normal probability plot’ for empirical probability versus ratios is shown in the lower panels [B1, B2, B3, and B4] of Fig. 11. This plot is a graphical representation of the normal distribution of ratios. The plot stays linear as long as the distributions are normal, and the deviation from the linear fit shows the divergence from the normal distribution. The solid line in the lower panels of Fig. 11 is between the 25th and 75th interquartile range of a ratio. The probability's grid (y-grid lines) is not linear and it is representative of the distance between quantiles of normal distribution.

The average, median, and standard deviations of ratios comparing GANDALF with other instruments are given in Table 4. The variation in these ratios (CRDS/GANDALF, CE-DOAS/GANDALF, and CLD/GANDALF) is small compared to LP-DOAS/GANDALF. This is expected as the LP-DOAS is not an in situ technique and instead measures an average concentration along the light path. The ratios CRDS / GANDALF and LP-DOAS/GANDALF are close to unity, whereas in the case of CE-DOAS/GANDALF and CLD/GANDALF they deviate from unity by 0.15. All ratios distribution generally show a trend close to a normal distribution (Fig. 11 [A1, A2, A3, and A4]) but the skewness in LP-DOAS / GANDALF (A1 in Fig. 11) on both sides of the average value is relatively largest. In the lower panel of Fig. 11 [B1, B2, B3, and B4], the probabilities show

525 a deviation from normality and a tail on top (towards the right) and bottom (towards the left) sides can be observed. The tail
could be an indicator of outliers, caused by for example the non-normality of the precision at low values, background level, and
potential interferences of NO₂ instruments. The lower panels [B1, B2, B3 and B4] of Fig. 11 show that a major fraction of the
ratios is normally distributed, evident from the 25th to 75th interquartile range of probability in all cases. The percentile of
530 probability towards normality is slightly greater (about 10th to 90th percentile) in the case of CLD/GANDALF compared to the
others. The percentile is about 15th to 80th and 25th to 90th with (CRD/GANDALF, CE-DOAS/GANDALF) and (LP-
DOAS/GANDALF), respectively. A perfect normal distribution should not be expected in these cases as mathematically a ratio
between two normally distributed quantities does not follow a normal-distribution but it can be a distribution like the Cauchy-
distribution (Weisstein, 2003). The long tails in the lower panel of Fig. 11 [B1, B2, B3, and B4] also indicates characteristics of
535 the Cauchy distribution. In this type of distribution, the accuracy of average and standard deviation values cannot be increase by
increasing the number of data points.

To identify systematic deviations based on other trace gases or parameters, ratios are further compared with the
observed data of several trace gases, radiation, and meteorological parameters. There are only two cases, where a systematic
correlation of ratios was observed with the observed quantities during PARADE, as shown in Fig. 12, and Fig. 13. In **Case 1**,
ratios are presented as a function of the observed O₃ concentrations. The ratio between CLD and GANDALF shows a decreasing
540 trend with respect to an increase in the O₃ concentrations (subplot **C4**, Fig. 12). This ratio (CLD/GANDALF) averages 0.95 at
levels less than 20 ppb O₃. It decreases to an average of 0.86 over the interval of 20 to 42 ppb O₃, while averaging 0.81 at levels
above 42 ppb of O₃. There is no trend observed in other ratios (CRDS/GANDALF, LP-DOAS/GANDALF, and CE-
DOAS/GANDALF) as shown in Fig. 12. The subplot (**C4**, Fig. 12) has been cross-checked by altering the GANDALF data in
the denominator to the other three measurements (LP-DOAS, CRDS, and CE-DOAS) and qualitatively similar trends were
545 observed as with GANDALF. The reason for this CLD/GANDALF trend is not clear at the moment. However, it seems that this
trend may be an indirect impact due to the zero-air measurement of the CLD with the BLC unit ON which is dependent on the
converter's history (exposition to ambient NO, NO₂, and HNO₃ concentrations along humidity) and potentially affect the
ambient NO₂ measurements. So the dependency on O₃ might be an indirect effect: high ozone could point to transport from
above with lower H₂O and lower NO_x, which both could affect the zero leading to an overestimation of the subtracted zero
550 signal. In **Case 2** (subplot **D3**, Fig. 13), a correlation is observed for the ratio between CE-DOAS/GANDALF as a function of
jNO₂. At higher values of jNO₂, the ratio approaches unity. The sampling line for CE-DOAS and CRDS was the same and no
correlation for the ratio between CRDS and GANDALF is seen with respect to jNO₂. However, the data for the CRDS
instrument was corrected for the effect of 'NO + O₃ → NO₂' in the sampling line and this correction for the CE-DOAS
instrument was not implemented. Hence, the jNO₂ trend in the ratio could be indirectly from 'NO + O₃'. A residence time of 10 s
555 in the sampling line for the 'NO + O₃ → NO₂' reaction (using measured NO, and O₃) is sufficient to explain this trend. This
correlation is also not observed for the ratios of LP-DOAS and CLD with respect to GANDALF. A cross check was done for
panel D3 (Fig. 13) by exchanging GANDALF in the denominator to three other measurements (LP-DOAS, CRDS, and CLD);
qualitatively similar trends were observed as previously. Besides the above-described systematic correlations, no indication of a
potential interference is obtained for any of the instruments.

560 **4 Summary**

The laser-induced fluorescence based instrument (GANDALF) has been developed for the measurement of atmospheric
NO₂. GANDALF has been tailored towards compact design with a low detection limit (5 – 10 ppt 1min⁻¹), and high precision

(0.5% + 3 ppt 1min⁻¹), making it capable of measuring NO₂ throughout the troposphere with a time resolution of ~~1-s to~~ 1 minute. The reliability of GANDALF was successfully tested during the PARADE-2011 field campaign. Several available NO₂ measurements based on different methods (absorption spectroscopy, chemiluminescence, and fluorescence) provided a unique chance of successful inter-comparison. ~~and most of the differences were under the uncertainties of individual measurements.~~ In general, all instruments performed well. GANDALF showed a very good correlation ($R^2 \approx 0.99$) in comparison to other in situ instruments (Fig. S11 in the supplement), and even with LP-DOAS the correlation was $R^2 \approx 0.9$. The differences in the absolute values were within the specified range of individual measurement errors. The main advantages and disadvantages of GANDALF compared to the other instruments are summarized as follows.

In comparison to the CRDS instrument, the main advantage for GANDALF is that the sampling can be achieved without an inlet-line. This is not possible for the close-path CRDS system. This provides the capability of the detection at ambient temperature for GANDALF, which is especially of an advantage for aircraft measurements of NO₂ where avoiding interference from CH₃OONO₂ and HO₂NO₂ (via unwanted thermal dissociation) is very important. The requirement of calibration is the main disadvantage for GANDALF compared to CRDS (absolute technique). However, both instruments require frequent zero-air measurements. The limit of detection for both instruments was of similar magnitude during PARADE-2011.

The CE-DOAS instrument is comparable to the CRDS instrument. It also needs frequent background measurements but no absolute calibration. GANDALF has a much better in the sensitivity compared to the CE-DOAS instrument. During PARADE-2011, the detection limit for CE-DOAS was around 300 ppt (2 σ , 30 s) while for GANDALF the detection limit was 5 – 10 ppt (min⁻¹). A low-cell-pressure is typically required to achieve a good sensitivity for LIF instruments (Table 1) while the detection in the other instruments (CRDS and CE-DOAS) is performed at sub-ambient pressures (>800 hPa). The requirement of calibration and usage of a larger scroll-pump (to achieve a low-cell-pressure) adds extra effort/cost to the GANDALF measurements.

The basic requirements for a calibration and background measurements are same in CLD and GANDALF. In the case of CLD, the maintenance is relatively easy compared to GANDALF. But GANDALF provides a direct detection of NO₂ compared to the indirect detection of NO₂ (via NO₂→NO) in the CLD instrument. The sensitivity of GANDALF was better than the CLD instrument during PARADE-2011.

LP-DOAS does not require calibration or the zero-air measurement. For this reason, the uncertainty of the data is also very small compared to GANDALF or other in situ measurements. This is the main advantage of the LP-DOAS instrument over GANDALF. The restriction of this method is that it does not provide a local measurement. Also, the temporal resolution is limited compared to other in situ instruments. The sensitivity of the LP-DOAS instrument generally depends on the length of a light path, and variations in visibility. It was on average about 110 ppt (2 σ , 11 s) during PARADE-2011.

The selectivity of NO₂ measurement with GANDALF compared to other measurements in ambient air was assessed during PARADE and no potential interference was found. This prototype could provide useful measurements of NO₂ under remote conditions where an interference-free detection is absolutely essential for the study of NO_x chemistry especially in the context of O₃ formation, and radical loss processes.

Outlook: NO₂ in the free troposphere is variable (seasonally) and generally lower than 50 ppt (Gil-Ojeda et al., 2015). Depending on the location, in the free troposphere and the marine boundary layer, NO₂ can be as low as a few ppt (Beygi et al., 2011;Schreier et al., 2016). These NO₂ ranges are below the detection limit for the instrument (GANDALF) for short time resolutions of 1s, for example. Improvements for future use on aircraft are possible by further reducing the background of the instrument. Since most of the background signal is from the fluorescence contamination of the Herriot's cell mirrors, this could be avoided by using a single beam (as demonstrated by (Di Carlo et al., 2013)) of the laser for detection without a Herriott cell or

by using different coatings on the Herriott cell mirrors to increase reflectivity and reduce fluorescence. The current CW diode laser of the instrument may be replaced by an already available mono-mode dual diode laser [λ (online) = 445 nm and λ (offline) = 442 nm] for on and off resonance measurements of NO₂. Replacement of the current laser by a dual diode laser will decrease partially the dependency on the frequent zero-air background measurements.

The formation of RONO₂ is an important sink for NO_x and effects the ozone production efficiency (Browne and Cohen, 2012). The accurate measurement of RONO₂ is important for the assessment of local O₃ abundances. LIF systems in combination with the thermal dissociation method (Day et al., 2002) are also used and very useful for the detection of RONO₂, RONO₂, and HNO₃. GANDALF will be capable (currently under development) of measuring these species by coupling with the thermal dissociation inlets. This further development could provide very useful data in the future to constrain models.

5 Acknowledgements

This work was done as a part of the first author's PhD, who is grateful for the constructive comments of Prof. P. Hoor during the PhD advisory committee meetings. The financial support from DFG (Deutsche Forschungsgemeinschaft) within the "DFG-Verfahren: Schwerpunktprogramm, SPP 1294: Bereich Infrastruktur - Atmospheric and Earth system research with the "High Altitude and Long Range Research Aircraft" (HALO)" is gratefully acknowledged. The authors are thankful to M. Tang, B. Bohn, F. Berkes, and G. Phillips, for the data of NO₃/N₂O₅, jNO₂, H₂O, and ClNO₂, respectively. The acknowledgement extends to K. Hens, A. Novelli, E. Regelin, C.T. Ernest, C. Mallik for the useful comments/logistics, the site engineers, DWD (Germany's National Meteorological Service) for meteorological data, and to the Goethe University, Frankfurt, for use of the Taunus Observatory facilities. We are thankful to the three anonymous referees for their comments and suggestions that helped us to improve the draft. We are also thankful to Lisa Whalley (editor) for the review process.

Data availability: Details about the field campaign can be found at <http://parade2011.mpich.de/>. The data related to PARADE-2011 can be obtained on request (by Hartwig Harder) from the responsible persons/owners.

Competing interests: There is no conflict of interests to declare.

6 References

Atkinson, R., Baulch, D. L., Cox, R. A., Crowley, J. N., Hampson, R. F., Hynes, R. G., Jenkin, M. E., Rossi, M. J., and Troe, J.: Evaluated kinetic and photochemical data for atmospheric chemistry: Volume I - gas phase reactions of O_x, HO_x, NO_x and SO_x species, Atmos Chem Phys, 4, 1461-1738, 2004.

Bekooy, J. P., Meerts, W. L., and Dymanus, A.: High-Resolution Laser-rf Spectroscopy on the A²Π_{3/2}-X²Π_{3/2} System of Iodine Oxide (IO), J Mol Spectrosc, 102, 320-343, Doi 10.1016/0022-2852(83)90044-9, 1983.

Bonn, B., Bourtsoukidis, E., Sun, T. S., Bingemer, H., Rondo, L., Javed, U., Li, J., Axinte, R., Li, X., Brauers, T., Sonderfeld, H., Koppmann, R., Sogachev, A., Jacobi, S., and Spracklen, D. V.: The link between atmospheric radicals and newly formed particles at a spruce forest site in Germany, Atmos. Chem. Phys., 14, 10823-10843, 10.5194/acp-14-10823-2014, 2014.

Bradshaw, J., Davis, D., Crawford, J., Chen, G., Shetter, R., Muller, M., Gregory, G., Sachse, G., Blake, D., Heikes, B., Singh, H., Mastromarino, J., and Sandholm, S.: Photofragmentation two-photon laser-induced fluorescence detection of NO₂ and NO: Comparison of measurements with model results based on airborne observations during PEM-Tropics A, Geophys Res Lett, 26, 471-474, Doi 10.1029/1999gl900015, 1999.

- 640 Browne, E. C., and Cohen, R. C.: Effects of biogenic nitrate chemistry on the NO_x lifetime in remote continental regions, *Atmos Chem Phys*, 12, 11917-11932, 2012.
- Burkholder, J. B., Talukdar, R. K., Ravishankara, A. R., and Solomon, S.: Temperature-Dependence of the HNO₃ UV Absorption Cross-Sections, *J Geophys Res-Atmos*, 98, 22937-22948, Doi 10.1029/93jd02178, 1993.
- 645 Butkovskaya, N., Kukui, A., and Le Bras, G.: HNO₃ forming channel of the HO₂+NO reaction as a function of pressure and temperature in the ranges of 72-600 torr and 223-323 K, *J Phys Chem A*, 111, 9047-9053, 10.1021/jp074117m, 2007.
- Cantrell, C. A.: Technical Note: Review of methods for linear least-squares fitting of data and application to atmospheric chemistry problems, *Atmos Chem Phys*, 8, 5477-5487, 2008.
- Cariolle, D., Evans, M. J., Chipperfield, M. P., Butkovskaya, N., Kukui, A., and Le Bras, G.: Impact of the new HNO(3)-forming channel of the HO(2)+NO reaction on tropospheric HNO(3), NO(x), HO(x) and ozone, *Atmos Chem Phys*, 8, 4061-4068, 2008.
- 650 Carpenter, L. J., Monks, P. S., Bandy, B. J., Penkett, S. A., Galbally, I. E., and Meyer, C. P.: A study of peroxy radicals and ozone photochemistry at coastal sites in the northern and southern hemispheres, *J Geophys Res-Atmos*, 102, 25417-25427, Doi 10.1029/97jd02242, 1997.
- Clapp, L. J., and Jenkin, M. E.: Analysis of the relationship between ambient levels Of O₃, NO₂ and NO as a function of NO chi in the UK, *Atmos Environ*, 35, 6391-6405, Doi 10.1016/S1352-2310(01)00378-8, 2001.
- 655 Cleary, P. A., Wooldridge, P. J., and Cohen, R. C.: Laser-induced fluorescence detection of atmospheric NO₂ with a commercial diode laser and a supersonic expansion, *Appl Optics*, 41, 6950-6956, Doi 10.1364/Ao.41.006950, 2002.
- Commane, R., Seitz, K., Bale, C. S. E., Bloss, W. J., Buxmann, J., Ingham, T., Platt, U., Pöhler, D., and Heard, D. E.: Iodine monoxide at a clean marine coastal site: observations of high frequency variations and inhomogeneous distributions, *Atmos Chem Phys*, 11, 6721-6733, DOI 10.5194/acp-11-6721-2011, 2011.
- 660 Crawford, J., Davis, D., Chen, G., Bradshaw, J., Sandholm, S., Gregory, G., Sachse, G., Anderson, B., Collins, J., Blake, D., Singh, H., Heikes, B., Talbot, R., and Rodriguez, J.: Photostationary state analysis of the NO₂-NO system based on airborne observations from the western and central North Pacific, *J Geophys Res-Atmos*, 101, 2053-2072, Doi 10.1029/95jd02201, 1996.
- Crutzen, P. J.: Role of NO and NO₂ in the Chemistry of the Troposphere and Stratosphere, *Annu Rev Earth Pl Sc*, 7, 443-472, DOI 10.1146/annurev.ea.07.050179.002303, 1979.
- 665 Dari-Salisburgo, C., Di Carlo, P., Giammaria, F., Kajii, Y., and D'Altorio, A.: Laser induced fluorescence instrument for NO₂ measurements: Observations at a central Italy background site, *Atmos Environ*, 43, 970-977, 10.1016/j.atmosenv.2008.10.037, 2009.
- Day, D. A., Wooldridge, P. J., Dillon, M. B., Thornton, J. A., and Cohen, R. C.: A thermal dissociation laser-induced fluorescence instrument for in situ detection of NO₂, peroxy nitrates, alkyl nitrates, and HNO₃, *J Geophys Res-Atmos*, 107, Artn 4046
670 10.1029/2001jd000779, 2002.
- 675 Di Carlo, P., Aruffo, E., Busilacchio, M., Giammaria, F., Dari-Salisburgo, C., Biancofiore, F., Visconti, G., Lee, J., Moller, S., Reeves, C. E., Bauguitte, S., Forster, G., Jones, R. L., and Ouyang, B.: Aircraft based four-channel thermal dissociation laser induced fluorescence instrument for simultaneous measurements of NO₂, total peroxy nitrate, total alkyl nitrate, and HNO₃, *Atmos Meas Tech*, 6, 971-980, 10.5194/amt-6-971-2013, 2013.
- Ehhalt, D. H., Rohrer, F., and Wahner, A.: Sources and distribution of NO_x in the upper troposphere at northern mid-latitudes *Journal of Geophysical Research: Atmospheres* (1984?2012) Volume 97, Issue D4, *Journal of Geophysical Research: Atmospheres* (1984-2012), 97, 3725-3738, 1992.
- 680 Fong, C., and Brune, W. H.: A laser induced fluorescence instrument for measuring tropospheric NO₂, *Review of Scientific Instruments*, 68, 4253, 10.1063/1.1148384, 1997.

- Fontijn, A., Sabadell, A. J., and Ronco, R. J.: Homogeneous Chemiluminescent Measurement of Nitric Oxide with Ozone - Implications for Continuous Selective Monitoring of Gaseous Air Pollutants, *Anal Chem*, 42, 575-579, Doi 10.1021/Ac60288a034, 1970.
- 685 Ge, B. Z., Sun, Y. L., Liu, Y., Dong, H. B., Ji, D. S., Jiang, Q., Li, J., and Wang, Z. F.: Nitrogen dioxide measurement by cavity attenuated phase shift spectroscopy (CAPS) and implications in ozone production efficiency and nitrate formation in Beijing, China, *J Geophys Res-Atmos*, 118, 9499-9509, Doi 10.1002/Jgrd.50757, 2013.
- George, L. A., and Obrien, R. J.: Prototype Fage Determination of NO₂, *Journal of Atmospheric Chemistry*, 12, 195-209, Doi 10.1007/Bf00048073, 1991.
- 690 Ghosh, B., Papanastasiou, D. K., Talukdar, R. K., Roberts, J. M., and Burkholder, J. B.: Nitryl Chloride (ClNO₂): UV/Vis Absorption Spectrum between 210 and 296 K and O(P-3) Quantum Yield at 193 and 248 nm, *J Phys Chem A*, 116, 5796-5805, Doi 10.1021/Jp207389y, 2012.
- Gottschaldt, K., Voigt, C., Jockel, P., Righi, M., Deckert, R., and Dietmuller, S.: Global sensitivity of aviation NO_x effects to the HNO₃-forming channel of the HO₂ + NO reaction, *Atmos Chem Phys*, 13, 3003-3025, 10.5194/acp-13-3003-2013, 2013.
- 695 Harwood, M. H., Jones, R. L., Cox, R. A., Lutman, E., and Rattigan, O. V.: Temperature-Dependent Absorption Cross-Sections of N₂O₅, *J Photoch Photobio A*, 73, 167-175, Doi 10.1016/1010-6030(93)90001-2, 1993.
- Harwood, M. H., Burkholder, J. B., Hunter, M., Fox, R. W., and Ravishankara, A. R.: Absorption cross sections and self-reaction kinetics of the IO radical, *J Phys Chem A*, 101, 853-863, Doi 10.1021/Jp962429b, 1997.
- 700 Herndon, S. C., Shorter, J. H., Zahniser, M. S., Nelson, D. D., Jayne, J., Brown, R. C., Miake-Lye, R. C., Waitz, I., Silva, P., Lanni, T., Demerjian, K., and Kolb, C. E.: NO and NO₂ emission ratios measured from in-use commercial aircraft during taxi and takeoff, *Environ Sci Technol*, 38, 6078-6084, Doi 10.1021/Es049701c, 2004.
- Herriott, D., Kompfner, R., and Kogelnik, H.: Off-Axis Paths in Spherical Mirror Interferometers, *Appl Optics*, 3, 523-&, Doi 10.1364/Ao.3.000523, 1964.
- 705 Hofzumahaus, A., Rohrer, F., Lu, K. D., Bohn, B., Brauers, T., Chang, C. C., Fuchs, H., Holland, F., Kita, K., Kondo, Y., Li, X., Lou, S. R., Shao, M., Zeng, L. M., Wahner, A., and Zhang, Y. H.: Amplified Trace Gas Removal in the Troposphere, *Science*, 324, 1702-1704, 10.1126/science.1164566, 2009.
- Horowitz, A., Meller, R., and Moortgat, G. K.: The UV-VIS absorption cross sections of the alpha-dicarbonyl compounds: Pyruvic acid, biacetyl and glyoxal, *J Photoch Photobio A*, 146, 19-27, Doi 10.1016/S1010-6030(01)00601-3, 2001.
- 710 Hosaynali Beygi, Z., Fischer, H., Harder, H. D., Martinez, M., Sander, R., Williams, J., Brookes, D. M., Monks, P. S., and Lelieveld, J.: Oxidation photochemistry in the Southern Atlantic boundary layer: unexpected deviations of photochemical steady state, *Atmos. Chem. Phys.*, 11, 8497-8513, 10.5194/acp-11-8497-2011, 2011.
- Keller-Rudek, H., Moortgat, G. K., Sander, R., and Sørensen, R.: The MPI-Mainz UV/VIS Spectral Atlas of Gaseous Molecules of Atmospheric Interest, *Earth Syst. Sci. Data*, 5, 365-373, 10.5194/essd-5-365-2013, 2013.
- 715 Kubistin, D., Harder, H., Martinez, M., Rudolf, M., Sander, R., Bozem, H., Eerdeken, G., Fischer, H., Gurk, C., Klupfel, T., Königstedt, R., Parchatka, U., Schiller, C. L., Stickler, A., Taraborrelli, D., Williams, J., and Lelieveld, J.: Hydroxyl radicals in the tropical troposphere over the Suriname rainforest: comparison of measurements with the box model MECCA, *Atmos Chem Phys*, 10, 9705-9728, DOI 10.5194/acp-10-9705-2010, 2010.
- Land, D. V., Levick, A. P., and Hand, J. W.: The use of the Allan deviation for the measurement of the noise and drift performance of microwave radiometers, *Measurement Science and Technology*, 18, 1917-1928, 10.1088/0957-0233/18/7/018, 2007.
- 720 Lelieveld, J., and Crutzen, P. J.: Influences of Cloud Photochemical Processes on Tropospheric Ozone, *Nature*, 343, 227-233, Doi 10.1038/343227a0, 1990.

- Lelieveld, J., Butler, T. M., Crowley, J. N., Dillon, T. J., Fischer, H., Ganzeveld, L., Harder, H., Lawrence, M. G., Martinez, M., Taraborrelli, D., and Williams, J.: Atmospheric oxidation capacity sustained by a tropical forest, *Nature*, 452, 737-740, 10.1038/nature06870, 2008.
- 725 Li, J. S., Reiffs, A., Parchatka, U., and Fischer, H.: In Situ Measurements of Atmospheric Co and Its Correlation with Nox and O-3 at a Rural Mountain Site, *Metrol Meas Syst*, 22, 25-38, 2015.
- Logan, J. A.: Nitrogen-Oxides in the Troposphere - Global and Regional Budgets, *J Geophys Res-Oc Atm*, 88, 785-807, Doi 10.1029/Jc088ic15p10785, 1983.
- 730 Martinez, M., Harder, H., Kubistin, D., Rudolf, M., Bozem, H., Eerdeken, G., Fischer, H., Klupfel, T., Gurk, C., Konigstedt, R., Parchatka, U., Schiller, C. L., Stickler, A., Williams, J., and Lelieveld, J.: Hydroxyl radicals in the tropical troposphere over the Suriname rainforest: airborne measurements, *Atmos Chem Phys*, 10, 3759-3773, 2010.
- Matsumi, Y., Murakami, S., Kono, M., Takahashi, K., Koike, M., and Kondo, Y.: High-sensitivity instrument for measuring atmospheric NO₂, *Anal Chem*, 73, 5485-5493, Doi 10.1021/Ac010552f, 2001.
- 735 Matsumoto, J., Hirokawa, J., Akimoto, H., and Kajii, Y.: Direct measurement of NO₂ in the marine atmosphere by laser-induced fluorescence technique, *Atmos Environ*, 35, 2803-2814, Doi 10.1016/S1352-2310(01)00078-4, 2001.
- Matsumoto, J., and Kajii, Y.: Improved analyzer for nitrogen dioxide by laser-induced fluorescence technique, *Atmos Environ*, 37, 4847-4851, 10.1016/j.atmosenv.2003.08.023, 2003.
- Meller, R., Raber, W., Crowley, J. N., Jenkin, M. E., and Moortgat, G. K.: The UV-Visible Absorption-Spectrum of Methylglyoxal, *J Photoch Photobio A*, 62, 163-171, Doi 10.1016/1010-6030(91)87017-P, 1991.
- 740 Molina, L. T., and Molina, M. J.: Ultraviolet-Absorption Spectrum of Chlorine Nitrite, *Clono, Geophys Res Lett*, 4, 83-86, Doi 10.1029/G1004i002p00083, 1977.
- Molina, L. T., and Molina, M. J.: Chlorine Nitrate Ultraviolet-Absorption Spectrum at Stratospheric Temperatures, *J Photochem*, 11, 139-144, Doi 10.1016/0047-2670(79)80047-7, 1979.
- 745 Mollner, A. K., Valluvadasan, S., Feng, L., Sprague, M. K., Okumura, M., Milligan, D. B., Bloss, W. J., Sander, S. P., Martien, P. T., Harley, R. A., McCoy, A. B., and Carter, W. P. L.: Rate of Gas Phase Association of Hydroxyl Radical and Nitrogen Dioxide, *Science*, 330, 646-649, 10.1126/science.1193030, 2010.
- Monks, P. S.: Gas-phase radical chemistry in the troposphere, *Chemical Society reviews*, 34, 376-395, 10.1039/b307982c, 2005.
- Newman, S. M., Howie, W. H., Lane, I. C., Upson, M. R., and Orr-Ewing, A. J.: Predissociation of the A²Π_{3/2} state of IO studied by cavity ring-down spectroscopy, *J Chem Soc Faraday T*, 94, 2681-2688, Doi 10.1039/A805103h, 1998.
- 750 Osthoff, H. D., Brown, S. S., Ryerson, T. B., Fortin, T. J., Lerner, B. M., Williams, E. J., Pettersson, A., Baynard, T., Dube, W. P., Ciciora, S. J., and Ravishankara, A. R.: Measurement of atmospheric NO₂ by pulsed cavity ring-down spectroscopy, *J Geophys Res-Atmos*, 111, Artn D12305, Doi 10.1029/2005jd006942, 2006.
- 755 Parra, J., and George, L. A.: Development of an ambient pressure laser-induced fluorescence instrument for nitrogen dioxide, *Appl Optics*, 48, 3355-3361, 2009.
- Perner, D., and Platt, U.: Detection of Nitrous-Acid in the Atmosphere by Differential Optical-Absorption, *Geophys Res Lett*, 6, 917-920, Doi 10.1029/G1006i012p00917, 1979.
- 760 Phillips, G. J., Tang, M. J., Thieser, J., Brickwedde, B., Schuster, G., Bohn, B., Lelieveld, J., and Crowley, J. N.: Significant concentrations of nitryl chloride observed in rural continental Europe associated with the influence of sea salt chloride and anthropogenic emissions, *Geophys Res Lett*, 39, Artn L10811, Doi 10.1029/2012gl051912, 2012.
- Platt, U., Perner, D., and Patz, H. W.: Simultaneous Measurement of Atmospheric CH₂O, O₃, and NO₂ by Differential Optical-Absorption, *J Geophys Res-Oc Atm*, 84, 6329-6335, Doi 10.1029/Jc084ic10p06329, 1979.

- Platt, U., and Stutz, J.: Differential Optical Absorption Spectroscopy, in, Springer-Verlag Berlin Heidelberg, 2008.
- 765 Platt, U., Meinen, J., Pöhler, D., and Leisner, T.: Broadband Cavity Enhanced Differential Optical Absorption Spectroscopy (CE-DOAS) - applicability and corrections, *Atmospheric Measurement Techniques*, 2, 713-723, 2009.
- Pöhler, D., Vogel, L., Friess, U., and Platt, U.: Observation of halogen species in the Amundsen Gulf, Arctic, by active long-path differential optical absorption spectroscopy, *Proc Natl Acad Sci U S A*, 107, 6582-6587, 10.1073/pnas.0912231107, 2010.
- 770 Reed, C., Evans, M. J., Di Carlo, P., Lee, J. D., and Carpenter, L. J.: Interferences in photolytic NO₂ measurements: explanation for an apparent missing oxidant?, *Atmos. Chem. Phys.*, 16, 4707-4724, 10.5194/acp-16-4707-2016, 2016.
- Riley, W. J.: A test suite for the calculation of time domain frequency stability, *Proceedings of the 1995 Ieee International Frequency Control Symposium*, 360-366, Doi 10.1109/Freq.1995.483922, 1995.
- Riley, W. J.: *Handbook of Frequency Stability Analysis*, National Institute of Standards and Technology (NIST), U.S. Department of Commerce, 136 pp., 2008.
- 775 Ryerson, T. B., Williams, E. J., and Fehsenfeld, F. C.: An efficient photolysis system for fast-response NO₂ measurements, *J Geophys Res-Atmos*, 105, 26447-26461, Doi 10.1029/2000jd900389, 2000.
- Sakurai, K., and Broida, H. P.: Spectral Study of No₂ Fluorescence Excited by 11 Lines of Argon and Krypton Ion Lasers, *J Chem Phys*, 50, 2404-&, Doi 10.1063/1.1671395, 1969.
- 780 Sander, S. P., Abbatt, J., Barker, J. R., Burkholder, J. B., Friedl, R. R., Golden, D. M., Huie, R. E., Kolb, C. E., Kurylo, M. J., Moortgat, G. K., Orkin, V. L., and Wine, P. H.: *Chemical Kinetics and Photochemical Data for Use in Atmospheric Studies*, in: JPL Publication 10-6, 2011.
- Sandholm, S. T., Bradshaw, J. D., Dorris, K. S., Rodgers, M. O., and Davis, D. D.: An Airborne Compatible Photofragmentation 2-Photon Laser-Induced Fluorescence Instrument for Measuring Background Tropospheric Levels of No, Nox, and No₂, *J Geophys Res-Atmos*, 95, 10155-10161, DOI 10.1029/JD095iD07p10155, 1990.
- 785 Seinfeld, J. H., and Pandis, S. N.: *Atmospheric Chemistry and Physics - From Air Pollution to Climate Change (2nd Edition)*, John Wiley & Sons, 2006.
- Singer, R. J., Crowley, J. N., Burrows, J. P., Schneider, W., and Moortgat, G. K.: Measurement of the Absorption Cross-Section of Peroxynitric Acid between 210 and 330 nm in the Range 253-298-K, *J Photoch Photobio A*, 48, 17-32, Doi 10.1016/1010-6030(89)87086-8, 1989.
- 790 Staffelbach, T. A., Orlando, J. J., Tyndall, G. S., and Calvert, J. G.: The Uv-Visible Absorption-Spectrum and Photolysis Quantum Yields of Methylglyoxal, *J Geophys Res-Atmos*, 100, 14189-14198, Doi 10.1029/95jd00541, 1995.
- Stavrakou, T., Muller, J. F., Boersma, K. F., van der A, R. J., Kurokawa, J., Ohara, T., and Zhang, Q.: Key chemical NO_x sink uncertainties and how they influence top-down emissions of nitrogen oxides, *Atmos Chem Phys*, 13, 9057-9082, 10.5194/acp-13-9057-2013, 2013.
- 795 Strand, A., and Hov, O.: The impact of man-made and natural NO_x emissions on upper tropospheric ozone: A two-dimensional model study, *Atmos Environ*, 30, 1291-1303, Doi 10.1016/1352-2310(95)00413-0, 1996.
- Sugimoto, N., Takezawa, S., and Takeuchi, N.: Time-Resolved, Dispersed Laser-Induced Fluorescence of NO₂ - Observation of Collision-Induced Energy-Transfer Effect, *Jpn J Appl Phys* 1, 21, 1536-1538, Doi 10.1143/Jap.21.1536, 1982.
- 800 Taketani, F., Kawai, M., Takahashi, K., and Matsumi, Y.: Trace detection of atmospheric NO₂ by laser-induced fluorescence using a GaN diode laser and a diode-pumped YAG laser, *Appl Optics*, 46, 907-915, Doi 10.1364/Ao.46.000907, 2007.
- Talukdar, R. K., Burkholder, J. B., Schmoltnner, A. M., Roberts, J. M., Wilson, R. R., and Ravishankara, A. R.: Investigation of the Loss Processes for Peroxyacetyl Nitrate in the Atmosphere - UV Photolysis and Reaction with OH, *J Geophys Res-Atmos*, 100, 14163-14173, Doi 10.1029/95jd00545, 1995.

- 805 Thieser, J., Schuster, G., Schuladen, J., Phillips, G. J., Reiffs, A., Parchatka, U., Pöhler, D., Lelieveld, J., and Crowley, J. N.: A two-channel thermal dissociation cavity ring-down spectrometer for the detection of ambient NO₂, RO₂NO₂ and RONO₂, *Atmos. Meas. Tech.*, 9, 553-576, 10.5194/amt-9-553-2016, 2016.
- Thornton, J. A., Wooldridge, P. J., and Cohen, R. C.: Atmospheric NO₂: In situ laser-induced fluorescence detection at parts per trillion mixing ratios, *Anal Chem*, 72, 528-539, Doi 10.1021/Ac9908905, 2000.
- 810 Vandaele, A. C., Hermans, C., Fally, S., Carleer, M., Colin, R., Merienne, M. F., Jenouvrier, A., and Coquart, B.: High-resolution Fourier transform measurement of the NO₂ visible and near-infrared absorption cross sections: Temperature and pressure effects, *J Geophys Res-Atmos*, 107, Artn 4348 Doi 10.1029/2001jd000971, 2002.
- Villena, G., Bejan, I., Kurtenbach, R., Wiesen, P., and Kleffmann, J.: Interferences of commercial NO₂ instruments in the urban atmosphere and in a smog chamber, *Atmospheric Measurement Techniques*, 5, 149-159, DOI 10.5194/amt-5-149-2012, 2012.
- 815 Washenfelder, R. A., Langford, A. O., Fuchs, H., and Brown, S. S.: Measurement of glyoxal using an incoherent broadband cavity enhanced absorption spectrometer, *Atmos. Chem. Phys.*, 8, 7779-7793, 10.5194/acp-8-7779-2008, 2008.
- Wayne, R. P., Barnes, I., Biggs, P., Burrows, J. P., Canosamas, C. E., Hjorth, J., Lebras, G., Moortgat, G. K., Perner, D., Poulet, G., Restelli, G., and Sidebottom, H.: The Nitrate Radical - Physics, Chemistry, and the Atmosphere, *Atmos Environ a-Gen*, 25, 1-203, Doi 10.1016/0960-1686(91)90192-A, 1991.
- 820 **Wehry, E. L.: Modern fluorescence spectroscopy, Modern analytical chemistry, Plenum Press, New York, v. <1-4 > pp., 1976.**
- Weisstein, E. W.: *CRC concise encyclopedia of mathematics*, 2nd ed., Chapman & Hall/CRC, Boca Raton, 3242 p. pp., 2003.
- Wojtas, J., Stacewicz, T., Bielecki, Z., Czyzewski, A., and Nowakowski, M.: NO₂ monitoring setup applying cavity enhanced absorption spectroscopy, *Eurocon 2007: The International Conference on Computer as a Tool*, Vols 1-6, 2152-2154, 2007.
- 825 York, D., Evensen, N. M., Martinez, M. L., and Delgado, J. D.: Unified equations for the slope, intercept, and standard errors of the best straight line, *Am J Phys*, 72, 367-375, 10.1119/1.1632486, 2004.

7 Tables

Table 1: Overview of different LIF instruments

Reference	$\lambda^{\text{laser type}}$ (nm)	Laser power (mW)	Absorption cross-section ($\times 10^{-19}$) cm ² molecule ⁻¹	Cell pressure (Pa)	LOD (ppt min ⁻¹)
(George and Obrien, 1991)	532 ¹	250	1.5	37	600
(Fong and Brune, 1997)	565 ²	250	0.6	1000	460
(Thornton et al., 2000)	585 ³	100-400	1	467	6
(Matsumi et al., 2001)	440 ⁴	100	7	35	12
(Matsumoto et al., 2001)	523.5 ⁵	360	1.4	93	125
(Cleary et al., 2002)	640.2 ⁶	16	3.9 ^C	27	145
(Matsumoto and Kajii, 2003)	532 ⁷	6500	1.5	267	4
(Taketani et al., 2007)	410 ⁸ , 473 ⁹	10, 15	6, 3	67	390, 140
(Parra and George, 2009)	406.3 ¹⁰	35	6	Ambient	2000 ^A
(Dari-Salisburgo et al., 2009)	532 ¹¹	8000-12000	1.5	60	12
(Di Carlo et al., 2013)	532¹²	38000	1.5	533	9.8 (s⁻¹)
GANDALF	447- 450 ¹³	Max. 200	5.3 ^E	700	5-10

^E Effective absorption cross-section; ^C Cooling enhancement; ^A Ambient pressure in the detection cell.

830 **Laser type** (Table 1 column 2)

¹ Nd: YAG laser; ² Copper vapour laser-pumped dye laser; ³ Pulsed YAG-pumped dye laser; ⁴ Optical parametric oscillator laser; ⁵ Nd: YLF laser harmonic; ⁶ External-cavity tunable diode laser; ⁷ Nd:YVO₄ pulse laser pumped by a solid-state laser; ⁸ GaN-based laser diode; ⁹ Diode-pumped Nd:YAG laser; ¹⁰ CW GaN semiconductor laser diode; ¹¹ YAG Q-switched intra-cavity doubled laser; ¹² **YAG Laser (Nd:YVO4 pulse laser)**; ¹³ CW diode laser

835

Table 2: NO₂ instruments located or sampling at the top of the platform during PARADE-2011.

Measurement (Operator)	Technique	Uncertainty	Detection Limit	Time resolution
LP-DOAS (IUP-HD)	Long Path DOAS	2 %	Avg.= 110 ppt (11s, 2σ)	13 s
CE-DOAS (IUP-HD)	Cavity-Enhanced DOAS	5 - 10 %	300 ppt (30 s, 2σ)	30-s 2 s
CRDS (MPIC)	Cavity Ring-Down Spectrometer	6 % ; 20 ppt	50 ppt (4s, 2 σ)	4 s
CLD (BLC) (MPIC)	Chemiluminescence Detector/ Blue light convertor	105 ppt; 10 %	55 ppt (2 s, 1 σ)	2 s
GANDALF (MPIC)	Laser-Induced Fluorescence	5 % + 11 ppt (1 σ)	5 - 10 ppt (1 min, SNR = 2)	1 s

840

Table 3: Fit parameters based on the bivariate model function according to the relation ($\text{NO}_2\text{Instruments} = a \times [\text{MedianNO}_2] + b$) at different NO_2 ranges. The value of $\text{NO}_2\text{Instruments}$ -intercept 'b' is in ppb. 'N' is number of data points and R^2 is the square correlation coefficient. $\pm \delta$ is the standard error of slope 'a' and intercept 'b'.

NO_2 Instruments	a	$\pm \delta_a$	b	$\pm \delta_b$	N	R^2	a	$\pm \delta_a$	b	$\pm \delta_b$	N	R^2
	$\text{NO}_2 < 1 \text{ ppb}$						$\text{NO}_2 \geq 1 \text{ to } \leq 6 \text{ ppb}$					
LP-DOAS	1.23	0.07	-0.15	0.05	208	0.80	1.03	0.008	-0.03	0.01	964	0.90
CE-DOAS	0.95	0.06	-0.06	0.05	208	0.80	0.92	0.01	-0.03	0.02	964	0.99
CRDS	1.1	0.07	-0.02	0.05	208	0.83	1.06	0.01	0.002	0.02	964	0.99
CLD	0.99	0.08	-0.12	0.06	208	0.73	0.97	0.01	-0.13	0.02	964	0.98
GANDALF	1.06	0.07	0.015	0.05	208	0.74	1.04	0.01	0.015	0.02	964	0.99
	$\text{NO}_2 > 6 \text{ to } < 12 \text{ ppb}$						$\text{NO}_2 \geq 12 \text{ ppb}$					
LP-DOAS	1.2	0.08	-1.51	0.6	52	0.64	1.42	0.2	-6.64	4	15	0.69
CE-DOAS	0.91	0.09	0.075	0.7	52	0.94	0.87	0.2	0.55	3	15	0.96
CRDS	1.09	0.09	-0.16	0.6	52	0.94	1.04	0.2	0.38	3	15	0.94
CLD	1.02	0.1	-0.64	0.7	52	0.81	0.89	0.2	0.51	3	15	0.84
GANDALF	1.05	0.08	0.016	0.6	52	0.94	0.99	0.2	0.52	3	15	0.94

845

Table 4: Average values of NO_2 ratios during PARADE-2011. These are derived from the different overall- NO_2 -measurements with respect to GANDALF overall- NO_2 -measurement.

Ratio	Average	Standard Deviation
LP-DOAS / GANDALF	0.96	0.19
CRDS / GANDALF	1.01	0.06
CE-DOAS / GANDALF	0.86	0.07
CLD / GANDALF	0.85	0.09

850

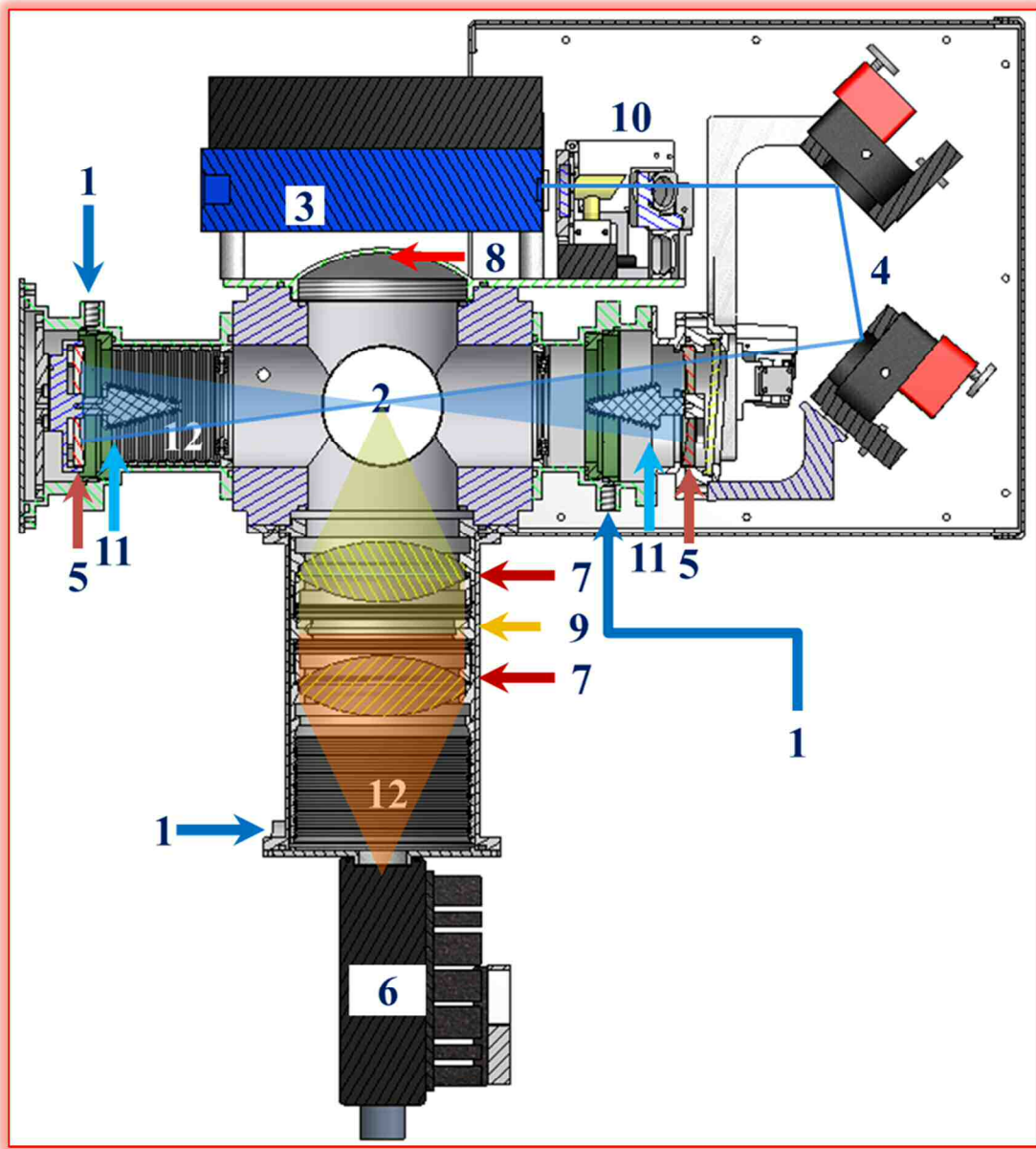
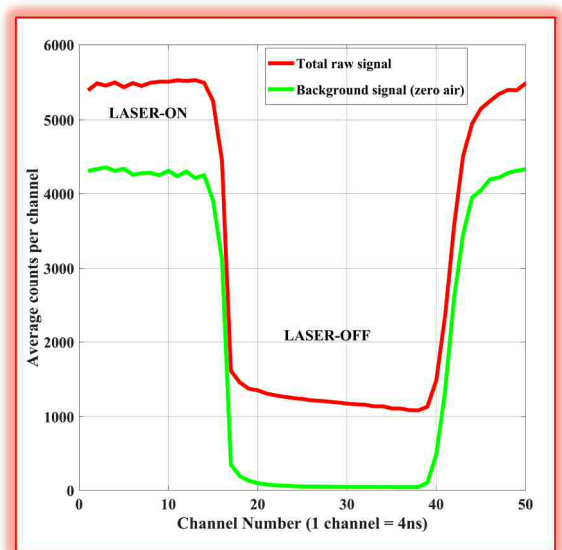
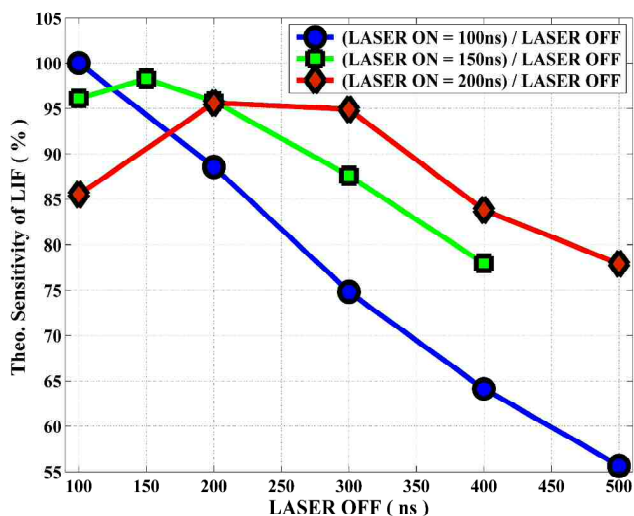


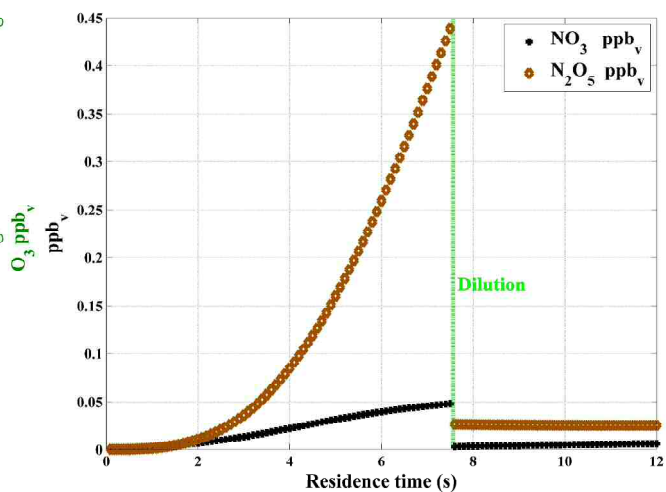
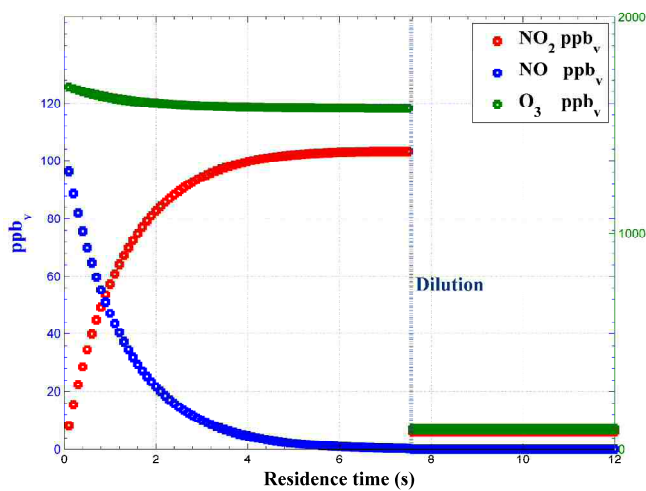
Figure 1: Section view²⁰ of GANDALF

(1): Flushing for optics (2): detection area (3): Diode laser (4): Motorised mirrors (5): Herriott cell's mirrors (6): PMT (7): Focusing lens (8): Concave mirror (9): Interference/optical filters (10): Optical reference system (11 and 12): Baffles

²⁰ Section view is based on Inventor-2009: The figure is created by defining a plane used to cut through the whole assembly. 3D AutoCAD models (1) for the diode laser by courtesy of Omicron Laserage Laserprodukte GmbH and (2) for optical mirror holders by courtesy of Newport.

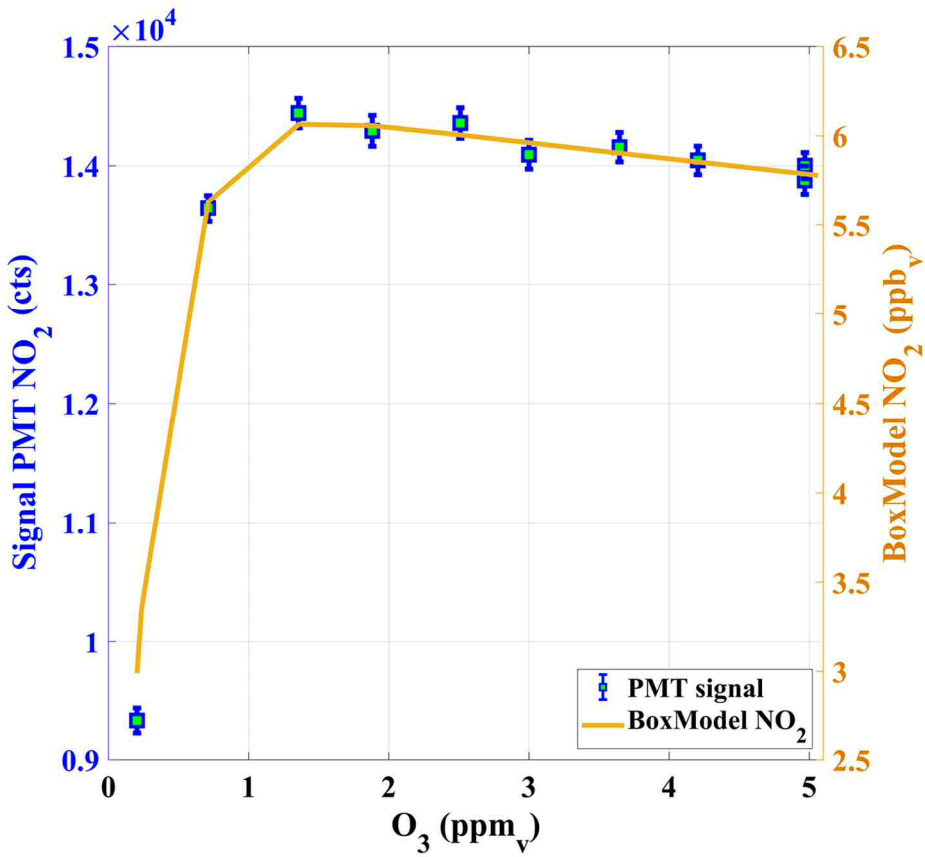


865 **Figure 2:** (Left-side): Relative sensitivity of the instrument based on simulation is demonstrated for three different on/off cycles of diode laser operation. (Right-side): ON-OFF cycle of the laser for a signal of about 12ppb NO₂ [y-axis arb. unit] is shown.

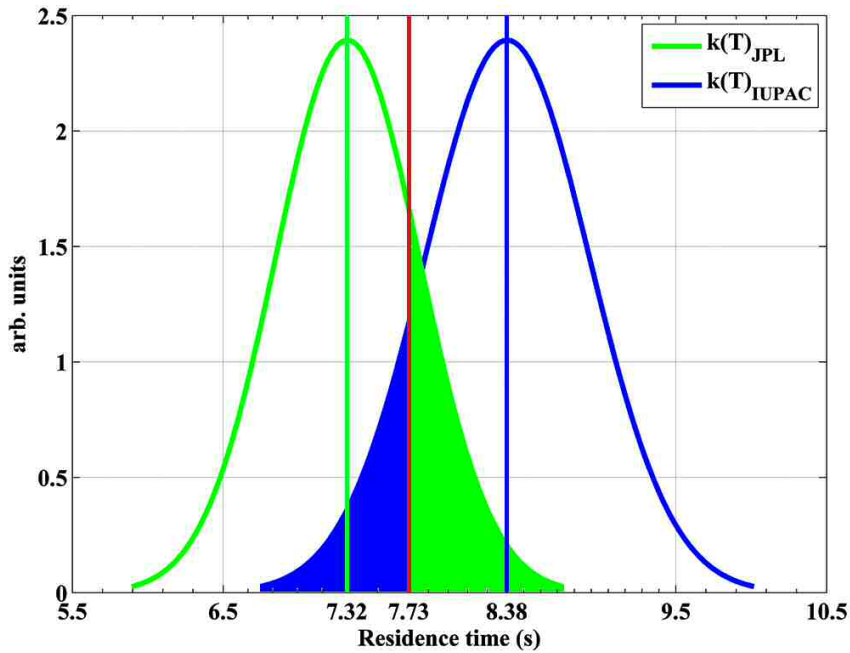


870 **Figure 3:** Box model simulation of gas phase titration of NO and O₃ (left panel) with loss of NO₂ due to formation of NO₃ and N₂O₅ (right panel).

875



880 **Figure 4: The PMT NO₂ signals in counts (cts) are shown as a function of O₃ concentrations in the calibrator (y-axis scale on the left side), together with NO₂ calculated from a box model of the NO₂ production in the calibrator (y-axis scale on the right side).**



885 **Figure 5: Residence time for NO₂ calibration gas in the calibrator based on Eq. 3. Also theoretically calculated residence time (7.73 s) is shown (red-line). The likelihoods (green or blue shaded areas) of residence times based on the JPL or IUPAC rate constant for being accurate are indistinguishable in comparison to the theoretically calculated residence time.**

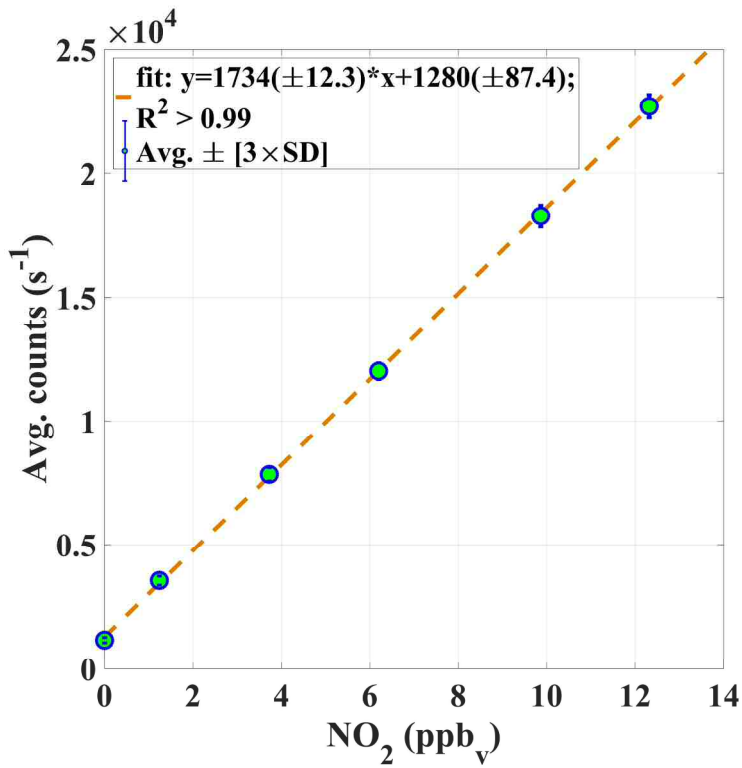


Figure 6: An example of the average PMT signal in counts (s^{-1}) vs known mixing ratios of NO_2 . The calibration constant α_c (Eq. 1) is given by the slope of the curve.

890

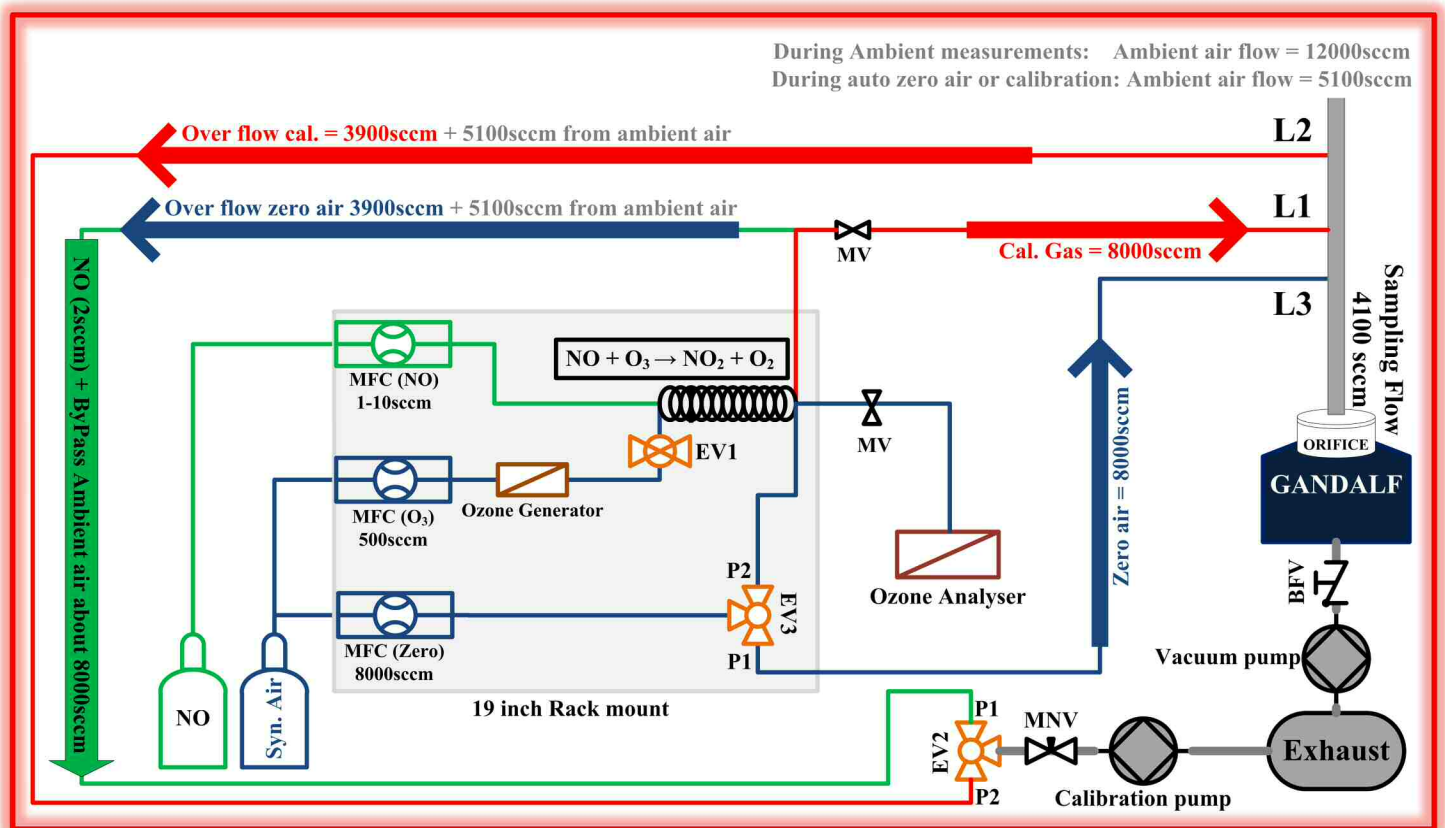
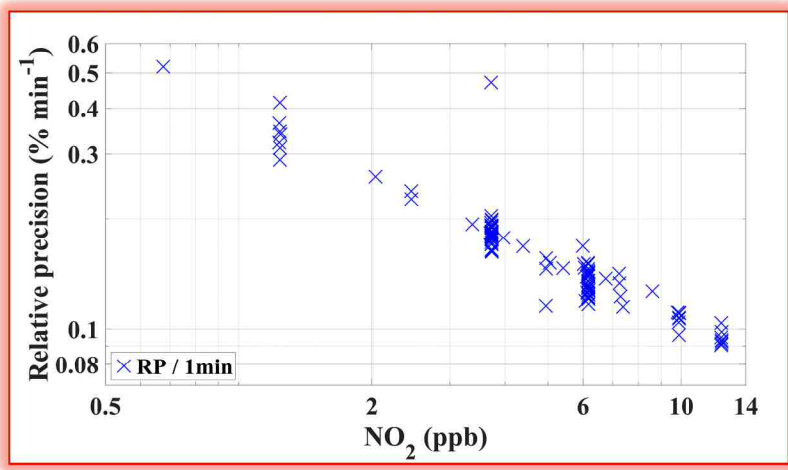
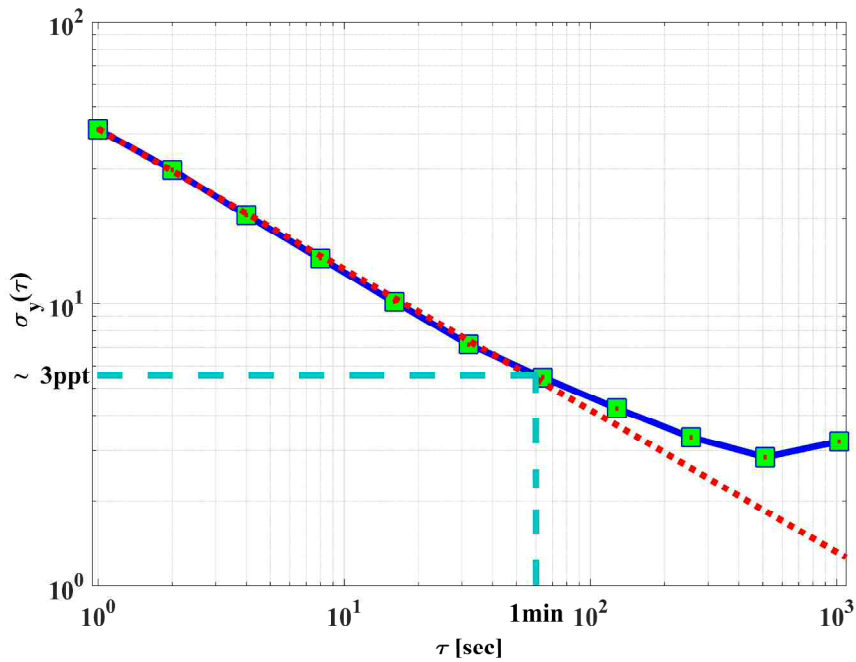


Figure 7: Schematic setup for the automated calibrations during PARADE-2011.



895 **Figure 8:** The relative precision in 1 minute of GANDALF is shown for PARADE-2011 as a function of NO₂ mixing ratios. The relative precision is calculated by randomly selected the PMT signal during a calibration period.



900 **Figure 9:** An overlapping Allan deviation plot for the dependence of the 1σ variation in the background signal vs. integration time. The red colour dotted line shows the square root dependency of the signal.

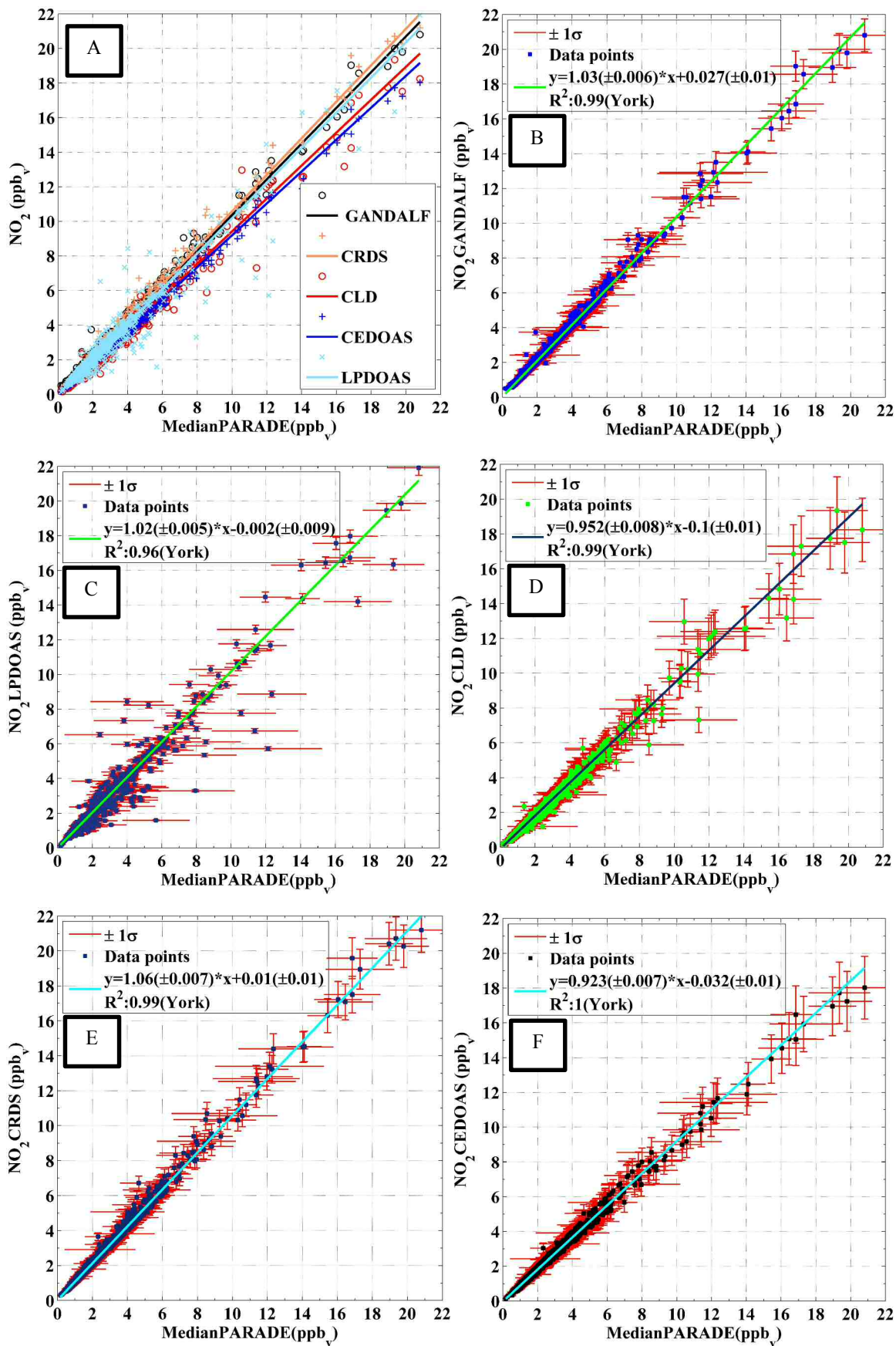
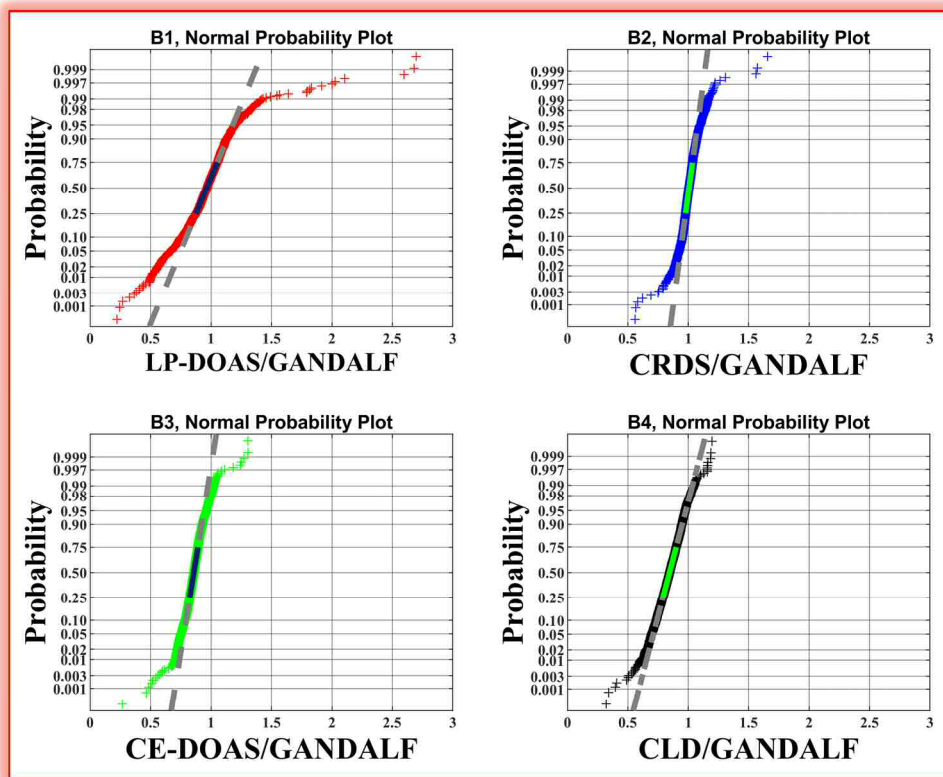
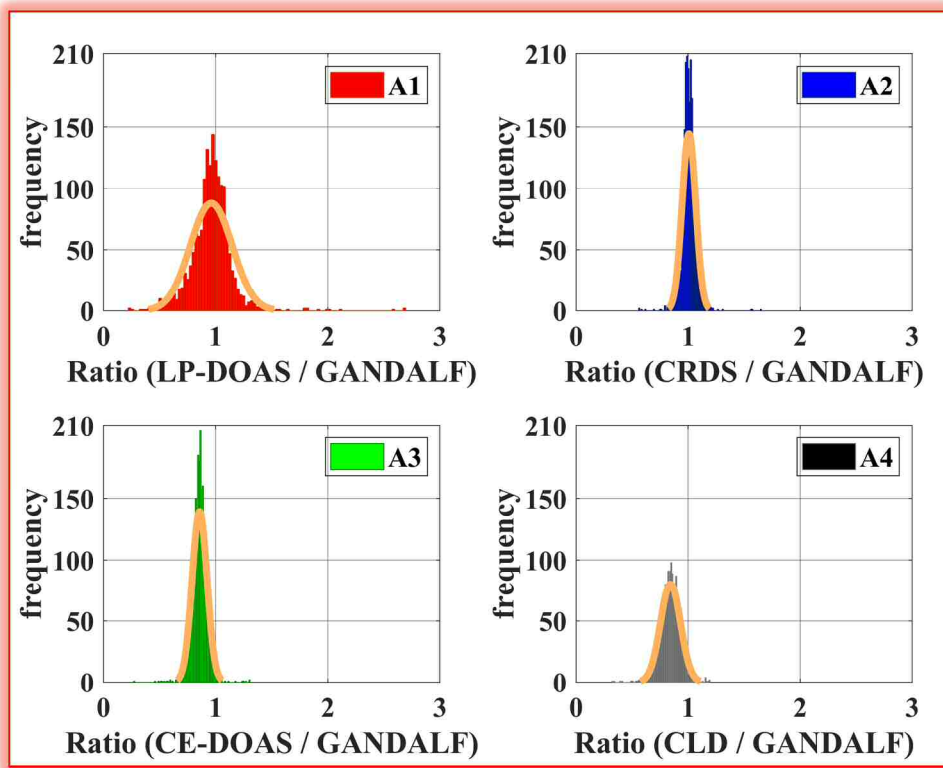


Figure 10: Correlation plots of individual NO_2 measurement versus the derived median values of all NO_2 measurement at the platform during PARADE. [A]: Overall, [B]: GANDALF, [C]: CLD, [D]: CRDS, [E]: LP-DOAS, [F]: CE-DOAS

905



5 Figure 11: Distribution of comparative instrument ratios of NO_2 measurements from different instruments is shown in upper panels (A1→A4) and a normal probability plot for comparative instrument ratios is shown in lower panels (B1→B4).

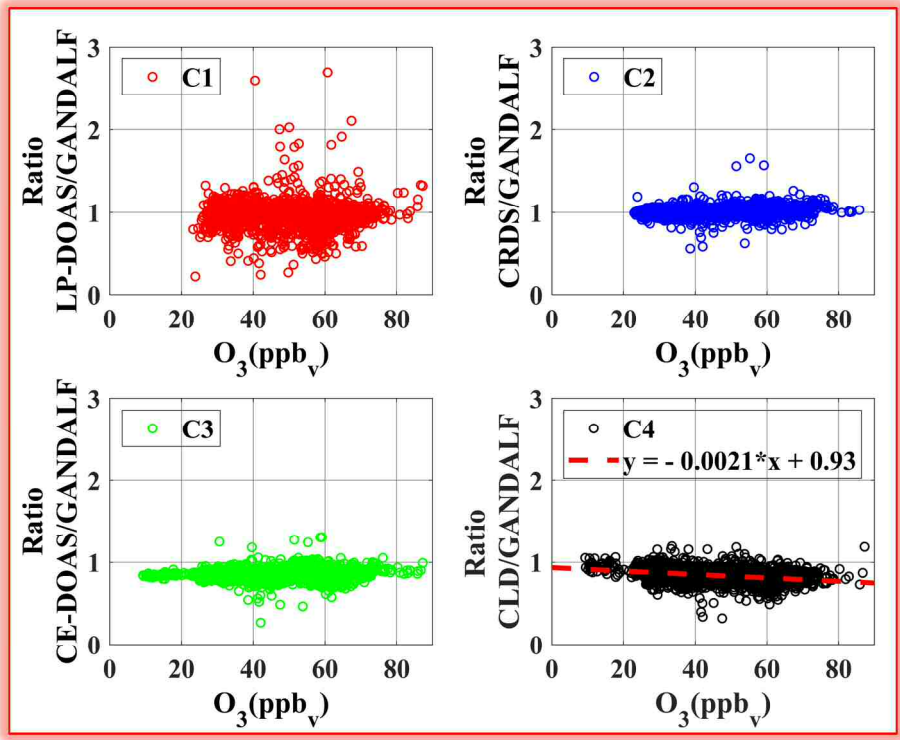


Figure 12: Ratios as a function of ambient O₃ during PARADE.

5

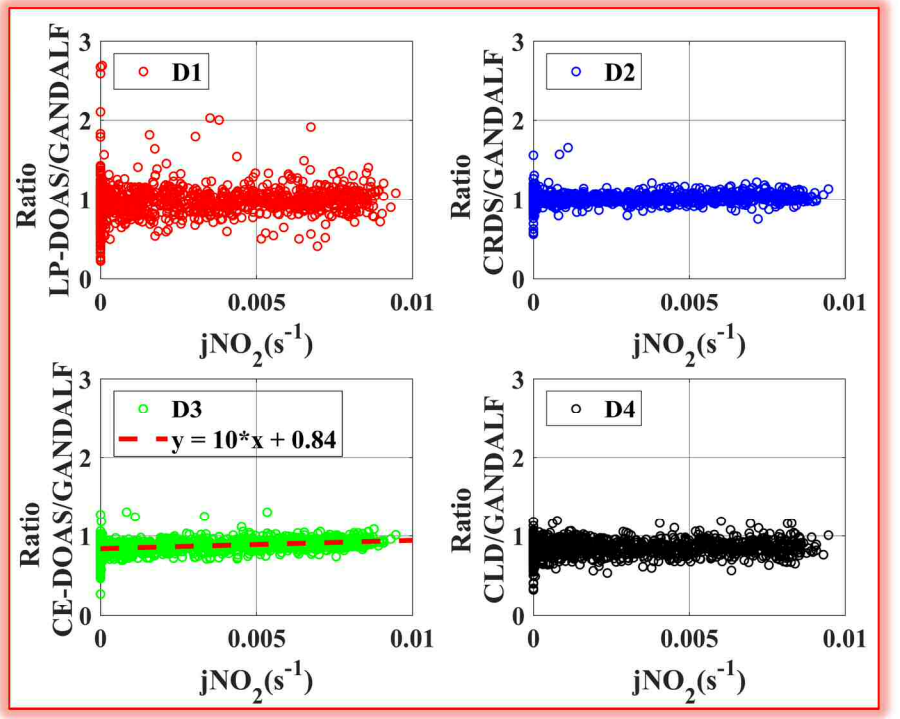


Figure 13: Ratios as a function of measured jNO₂ during PARADE.